Carderock Division, Naval Surface Warfare Center

West Bethesda, Maryland 20817-5700

NSWCCD-50-TR-2011/016 March 2011

Hydromechanics Department Report

Summary of Two Independent Performance Measurements of the ONR Axial Waterjet 2 (AxWJ-2)

by

Matthew W. Marquardt

20110412262

REPORT DOCUMENTATION PAGE

Form Approved

OMB No. 0704-0188

Public reporting burden for this collection of information is estimated to average 1 hour per response, including the time for reviewing instructions, searching existing data sources, gathering and maintaining the data needed, and completing and reviewing this collection of information. Send comments regarding this burden estimate or any other aspect of this collection of information, including suggestions for reducing this burden to Department of Defense, Washington Headquarters Services, Directorate for Information Operations and Reports (0704-0188), 1215 Jefferson Davis Highway, Suite 1204, Arlington, VA 22202-4302. Respondents should be aware that notwithstanding any other provision of law, no person shall be subject to any penalty for failing to comply with a collection of information if it does not display a currently valid OMB control number. **PLEASE DO NOT RETURN YOUR FORM TO THE ABOVE ADDRESS.**

1. REPORT DATE March 2011	2. REPORT TYPE Technical	3. DATES COVERED 11/2010-12/2010

4. TITLE AND SUBTITLE	5a. CONTRACT NUMBER
Summary of Two Independent Performance Measurements of the ONR Axial Waterjet 2 (AxWJ-2)	5b. GRANT NUMBER
	5c. PROGRAM ELEMENT NUMBER

6. AUTHOR(S)	5d. PROJECT NUMBER
Matthew W. Marquardt	5e. TASK NUMBER
	5f. WORK UNIT NUMBER 10-1-5800-330

7. PERFORMING ORGANIZATION NAME(S) AND ADDRESS(ES) AND ADDRESS(ES)	8. PERFORMING ORGANIZATION REPORT NUMBER
Naval Surface Warfare Center Carderock Division 9500 Macarthur Boulevard West Bethesda, MD 20817-5700	NSWCCD-50-TR-2011/016

9. SPONSORING / MONITORING AGENCY NAME(S) AND ADDRESS(ES)	10. SPONSOR/MONITOR'S ACRONYM(S)
Office of Naval Research 331 Ship Systems and Engineering Research Division 875 North Randolph Street Arlington, Virginia 22203	ONR 331
	11. SPONSOR/MONITOR'S REPORT NUMBER

12. DISTRIBUTION / AVAILABILITY STATEMENT

Approved for public release. Distribution Unlimited.

13. SUPPLEMENTARY NOTES

14. ABSTRACT

This report presents the experimental axial flow waterjet measurements of the ONR AxWJ-2, conducted by Rolls Royce Naval Marine and the Naval Surface Warfare Center Carderock Division. While the details and the data of these two experiments can be found in separate reports, the purpose of this document is to provide an all-in-one comparison of their findings, to be used by researchers across the hydrodynamic field in the public domain. This report aims at providing waterjet information to those in both the experimental and computational fluid dynamic realms to establish the ONR AxWJ-2 as a benchmark design, to further the development of waterjet-related design and analysis tools, and for validation purposes. Discussion is provided regarding each facilities geometry, setup, and measurement techniques. Comparisons are made between the datasets highlighting disparities in the results. Differences between the results were attributed to Reynolds scaling effects, rotor tip clearance, and testing procedures.

15. SUBJECT TERMS: Waterjet

16. SECURITY CLASSIFICATION OF:			17. LIMITATION OF ABSTRACT	18. NUMBER OF PAGES	19a. NAME OF RESPONSIBLE PERSON Matthew W. Marquardt
a. REPORT UNCLASSIFIED	b. ABSTRACT UNCLASSIFIED	c. THIS PAGE UNCLASSIFIED	Unlimited	46	19b. TELEPHONE NUMBER (301) 227-4878

Standard Form 298 (Rev. 8-98)

Prescribed by ANSI Std. Z39.18

(THIS PAGE INTENTIONALLY LEFT BLANK)

Contents

Tables

Figures

Symbols

A_n	Cross sectional area of casing, minus shaft or hub area, at station n
c	Rotor blade chord
D, D_3	Diameter of the inlet
D_6	Diameter of the nozzle exit
g	Gravitational constant
H	Total head rise, $H = p_{t6} - p_{t3}$
H^*	Head coefficient, $H^* = \dfrac{p_{t6} - p_{t3}}{\rho n^2 D^2}$
n	Revolutions per second
N^*	Cavitation coefficient, $N^* = \dfrac{p_{t3} - p_v}{\rho n^2 D^2} = \dfrac{g \cdot NPSH}{n^2 D^2}$
$NPSH$	Net positive suction head, $NPSH = \dfrac{p_{t3} - p_v}{\rho g}$
p_n	Static pressure at station n
p_{tn}	Total pressure at station n, $p_{tn} = p_n + \beta_{E\,n} \cdot \dfrac{1}{2}\rho\left(\dfrac{Q_J}{A_n}\right)^2$
p_v	Vapor pressure of water
P_d	Shaft power, $P_d = \dfrac{Q\,n}{550}$
P^*	Power coefficient, $P^* = \dfrac{2\pi\,n\,Q}{\rho n^3 D^5}$
Q	Torque
Q_J	Volumetric flow rate
Q^*	Flow coefficient, $Q^* = \dfrac{Q_J}{nD^3}$
r	Propeller radius at a section
R	Overall propeller radius
Re_{rotor}	Rotor Reynolds number, $Re_{rotor} = \dfrac{c_{70\%span}\sqrt{U_x^2 + (0.7\pi n D)^2}}{\upsilon}$
Re_{inlet}	Reynolds number, based on inlet diameter, $Re_{inlet} = \dfrac{DU_x}{\upsilon}$
U_x	Mean axial velocity
u_x, u_t, u_r	Axial, tangential, and radial velocity components
x, y, z	Axial, transverse, and vertical coordinates
$\beta_{E\,n}$	Energy non-uniformity factor, at station n
η	Pump efficiency
θ	Circumferential coordinate
ν	Kinematic viscosity
ρ	Mass density

Abbreviations

ONR AxWJ-2	ONR Axial Flow Waterjet 2
NSWCCD	Naval Surface Warfare Center, Carderock Division
ONR	Office of Naval Research
rpm	Revolutions per minute
RRHRC	Rolls-Royce Hydrodynamic Research Center
RRNMI	Rolls-Royce Naval Marine Incorporated
36VPWT	36-inch Variable Pressure Water Tunnel

Abstract

This report presents the experimental axial flow waterjet measurements of the ONR AxWJ-2, conducted by Rolls Royce Naval Marine and the Naval Surface Warfare Center Carderock Division. While the details and the data of these two experiments can be found in separate reports, the purpose of this document is to provide an all-in-one comparison of their findings to be used by researchers across the hydrodynamic field in the public domain. This report aims at providing waterjet information to those in both the experimental and computational fluid dynamic realms to establish the ONR AxWJ-2 as a benchmark design, to further the development of waterjet-related design and analysis tools, and for validation purposes. Discussion is provided regarding each facilities geometry, setup, and measurement techniques. Comparisons are made between the datasets highlighting disparities in the results. Differences between the results were attributed to Reynolds scaling effects, rotor tip clearance, and testing procedures.

Administrative information

Introduction

The ONR AxWJ-2 design and test program emerged from the need to have a waterjet geometry and data available to the general hydrodynamic community for evaluation purposes. Previously, relevant waterjet designs and data were proprietary. Public domain details and data of the ONR AxWJ-2 serves as a benchmark and forms a foundation to build on new designs and analysis tools. The collaborative study of this common waterjet brings greater focus to Navy-related waterjet research and will accelerate the development process of waterjets for use in large combatant vessels. The purpose of this report is to compare and validate test results of the ONR AxWJ-2 from two independent research groups.

In 2006, ONR started a program to develop a compact and high-power-density waterjet. ONR made a call for waterjet designs in a Broad Agency Announcement, ONR BAA06-011.[1] In 2008, ONR tasked the Naval Surface Warfare Center Carderock Division, NSWCCD, to design the ONR AxWJ-2. The geometry, hydrodynamic aspects, and other design considerations of the waterjet are documented by Michael et al.[2] Following the waterjet's inception, it was tested in two independent water tunnel experiments, carried out by

---

[1] References are on page 36

NSWCCD[3] and RRNMI.[4] The waterjet models of NSWCCD and RRNMI were geosyms with an inlet diameter of 12 in. (304.8 mm) and 7.87 in. (200 mm) respectively. The joint experimental tests provide the Navy with insight as to how waterjets are evaluated and measured by the vendors. Also, it enables comparisons to be drawn between the Navy's facilities and those of it vendors to identify potential biases. The objectives of this report are to summarize the findings of NSWCCD and RRNMI, provide a database of ONR AxWJ-2 experimental data, and to compare and contrast results. This database would offer easy-to-access knowledge used for prediction, benchmarking, and validation purposes.

Test procedures and methodology

The main objective of the RRNMI and NSWCCD tests were to quantify powering performance and cavitation characteristics in uniform inflow. Powering performance was evaluated at non-cavitating conditions through measurements of flow rate, rotor shaft speed, torque, and head rise. Cavitation was assessed making these same powering measurements, while at the same time, the test section pressure of the water tunnel was adjusted to advance or retard cavitation. Bubbly cavitation regions were documented using photographs and video. Several additional measurements were conducted and included flow field surveys, comprehensive thrust breakdown analysis, and cavitation videos.

Waterjet

The 6-bladed rotor and 8-bladed stator waterjet was designed for model testing, but is based on requirements for a notional high speed ship. The assumed characteristics of the ship were a delivered rotor shaft power of 27,500 hp (20,560 kW), top speed of 50 knots (26 m/s), an inlet diameter of 67 in. (1.7 m.)., wake fraction of 0.9, and thrust deduction of 1.09. The ratio of the inlet cross sectional area, minus the hub area, to the exhaust area is 1.85. The intended operating point of the waterjet was a flow coefficient of $Q^* = 0.85$ and a notional jet velocity (nozzle velocity) to wake speed (the product of the ship speed and the wake fraction) ratio of 1.5. The waterjet geometry is designed for model testing in two ways: first, the rotor to stator spacing is enlarged by 1 inch (25 mm) for flow surveys aft of the rotor, and second, the nozzle is lengthened to generate a uniform pressure at the nozzle exit. An illustration of the waterjet is shown in Figure 1.

The waterjets of the NSWCCD and RRNMI are geosyms in all but one respect, the tip gap spacing between the rotor and casing is different. The NSWCCD waterjet has a tip gap of 0.02 inches (0.51 mm), an amount smaller than the side-to-side play in the rotor shaft, to avoid rotor to casing contact. The RRNMI waterjet has a tip gap spacing of 0.01 inches (0.25 mm), geometrically proportional to the full-scale tip gap. The ratio of the tip gap to rotor diameter for the NSWCCD geosym is 0.00167, compared to 0.00125 for the RRNMI geosym.

Specifications and dimensions of the waterjet and the dimensions of the RRNMI and NSWCCD geosyms are listed in Table 1. To establish common definitions of waterjet locations, the naming conventions of the 21st ITTC Quality Manual[5] are adopted. The locations of the ITTC stations are shown in Figure 2. The locations referred to in this report are:

Station 3:   Just ahead of the rotor blade tips, or at the pump inlet flange

Station 4:   Between the rotor and the stator

Station 5:   Just aft of the pump stator or at the pump discharge flange

Station 6:   At the nozzle outlet plane

Station 7:   Aft of the nozzle

The specific locations of the stations relative to the ONR AxWJ-2 are shown in Figure 3. A fixed Cartesian coordinate system is established at the intersection of the shaft centerline and the forward face of the rotor hub. The origin is located between stations 3 and 4, with axes aligned with the shaft centerline. The x-, y-, and z-axes are normalized by the inlet radius, and extend downstream, transversely to port, and downward respectively. An illustration of the coordinate system appears in Figure 3. At times a polar coordinate system is used, having the same origin and x-axis, but with a radial coordinate r and angular coordinate θ. The coordinate θ originates from the top center and rotates clockwise when viewed from upstream, opposite of the rotor rotation.

Facilities and coordinate system

Code 5800, Resistance and Propulsion Division of the NSWCCD, tested the waterjet in the 36-inch variable pressure water tunnel. The closed loop tunnel was configured with the open jet test section. All the water directed to the test section is channeled through a bellmouth to the waterjet inlet. Configurable waterjet exhaust nozzles and downstream orifices provide back pressure to adjust the operating point of the pump. The flow rate is further adjusted by the water tunnel impeller. The Rolls-Royce Hydrodyanmic Research Center, located in Kristinehamn, Sweden, tested the waterjet in their closed loop and closed test section cavitation channel, called T-32. Unlike the NSWCCD, only some of the water in the test section is ingested by the waterjet. The exhaust flow is ducted to a pipe system, external of the test section, featuring auxiliary pumps and a flow meter; exhaust water is returned to the tunnel thereafter. A side-by-side illustration of the facilities and waterjet setup is shown in Figure 4.

Test conditions

The test conditions at each facility varied depending on the measurement. There are three categories of measurements: powering, velocity surveys, and thrust breakdown/cavitation. A summary of the test conditions, measurements, and measurement locations are documented in Table 2. Total inlet pressures for powering and

velocity survey tests were in the range of 35 to 50 psia (241 to 345 kPa). RRNMI ran powering and velocity survey tests at a rotor speed of 1200 rpm, and thrust breakdown and cavitation tests at 1350 rpm. Similarly, NSWCCD performed powering and velocity survey tests at 1400 rpm, and thrust breakdown and cavitation tests at 2000 rpm. At the design flow coefficient of $Q^* = 0.85$, RRNMI tests were run at a flow rate of 4.81 ft^3/s (0.136 m^3/s), a head rise of 4.90 psi (33.9 kPa), and torque of 31.5 ft-lbs (42.8 Nm). At the same design flow coefficient, NSWCCD tests were run at a flow rate of 19.8 ft^3/s (0.560 m^3/s), head rise of 15.7 psi (108. kPa), and torque of 351 ft-lbs (176 Nm). For the design flow coefficient of $Q^* = 0.85$, the Reynolds number based on inlet diameter was $8.72 \cdot 10^5$ for RRNMI tests and $3.22 \cdot 10^6$ for NSWCCD tests; similarly the respective rotor Reynolds numbers were $1.53 \cdot 10^6$ and $5.36 \cdot 10^6$.

Thrust breakdown and cavitation measurements were used to characterize how cavitation affects powering performance. Thrust breakdown is determined by operating the pump at constant rpm and decreasing the tunnel pressure until torque, head rise, and efficiency drop off. Thrust breakdown measurements are generally performed at a constant flow rate. RRNMI was able to maintain flow rate without the aid of the tunnel impeller using an auxiliary pump. NSWCCD would encounter a decreasing flow rate at low tunnel pressures because of cavitation concerns on the tunnel impeller.

Data reduction methodology

Powering relations

The flow rate Q_j, is non-dimensionalized and represented as the flow coefficient Q^*, given by

$$Q^* = \frac{Q_J}{nD^3} \tag{1}$$

where n denotes the rotor speed and D is the rotor diameter. Similarly, torque Q, is non-dimensionalized and takes the form of the power coefficient P^*, which is expressed as

$$P^* = \frac{2\pi Q}{\rho n^2 D^5} = 2\pi K_Q \quad \text{where} \quad K_Q = \frac{Q}{\rho n^2 D^5} \tag{2}$$

The total head rise across the pump is determined from head measurements at the inlet, station 3, and at the nozzle, station 6. The total head, $p_{\beta\,t\,n}$, at station n, is the sum of the static, $p_{stat\,n}$, and dynamic, $p_{\beta\,dync\,n}$, head components given by

$$p_{\beta\,tn} = p_{stat\,n} + p_{\beta\,dync\,n} = p_{stat\,n} + \beta_{E\,n}\frac{1}{2}\rho\left(\frac{Q_J}{A_n}\right)^2 \quad n = 3 \text{ or } 6 \tag{3}$$

where the term, $\beta_{E\,n} \cdot \tfrac{1}{2}\rho(Q_j/A_n)^2$ is the dynamic head; ρ is the water density, A_n is the cross sectional area of the

4

casing minus the hub or shaft area, and n denotes the station number. The term $\beta_{E\,n}$, is the energy non-uniformity factor and relates the mass-averaged dynamic pressure to the dynamic pressure calculated from the average velocity. The energy non-uniformity factor is defined as

$$\beta_{En} = \frac{1}{A} \int \frac{u_x RSS(u_x,u_t,u_r)^2}{U_x^{\,3}} dA \quad n = 3 \text{ or } 6 \tag{4}$$

where u_x is the axial velocity, U_x is the mean axial velocity, and the term $RSS(u_x, u_t, u_r)$ is the velocity magnitude computed from the root sum square of the axial, tangential, and radial velocity components. The energy non-uniformity factor approaches unity for purely axial flow and is greater than one for all other flows.

The energy non-uniformity factor is one method to account for dynamic losses at a station, but other techniques exist. RRNMI does not use β_E, but uses its own correction procedures. RRNMI does not provide enough information to determine exactly how the corrections are made, nor can one infer an equivalent β_E. An important point to note, RRNMI measures the total head at roughly two rotor radii downstream of the nozzle at station 7 – not station 6. Part of RRNMI correction procedure is to calculate the pressures loss incurred between station 6 and 7, and add this to their static pressure to emulate the total head at station 6. The author stipulates that RRNMI measures total head at station 7 because the swirl in the exhaust flow is reduced compared to station 6; swirl has the adverse affect of causing a non-uniform pressure field, varying in the radial direction, resulting in erroneously elevated static wall pressures. However, the RRNMI correction procedure includes a provision to remove this swirl-related pressure from the static pressures measurements – yet swirl is measured at station 7 diminished levels. The remaining feature of RRNMI correction procedure is to calculate the term $\frac{1}{2}\rho(Q_j/A_n)^2$ using a slightly smaller area then the actual area to account for the boundary layer displacement thickness.

Total head values are also calculated omitting corrections, and are denoted $p_{t\,n}$ and $p_{dync\,n}$ respectively. If corrections were made to the total head at stations 3 and 6, the corrected head rise, H_{corr}, is calculated by

$$H_{corr} = p_{\beta t6} - p_{\beta t3} \quad (\text{or } H_{corr} = p_{\beta t7} - p_{\beta t3} \text{ in the case of RRNMI}) \tag{5}$$

When omitting corrections, the head rise, H, is given by

$$H = p_{t6} - p_{t3} \quad (\text{or } H = p_{t7} - p_{t3} \text{ in the case of RRNMI}) \tag{6}$$

Both H_{corr} and H can be nondimensionalized, and are then called the corrected head coefficient and the head coefficient, respectively. These coefficients are nondimensionalized in the following manner

$$H^*_{corr} = \frac{H_{corr}}{\rho\, n^2 D^2} \tag{7}$$

$$H^* = \frac{H}{\rho\, n^2 D^2} \tag{8}$$

5

The waterjet efficiency is calculated from the quotient of the flow, power, and head coefficients; they are shown in the corrected form η_{corr}, and plain form η, as

$$\eta_{corr} = \frac{Q^* H_{corr}^*}{P^*} \tag{9}$$

$$\eta = \frac{Q^* H^*}{P^*} \tag{10}$$

Velocity relations

Velocity measurements at the inlet, station 3, are important to identify if nonuniformities exists in the inflow and the thickness of the shafting and casing boundary layers. Velocity measurements at stations 6 and 7 are used to detect swirl, wakes, and vortex structures emitted from the waterjet. Velocity measurements are normalized by either the mean axial velocity at the inlet, U_{x3}, or the tip rotational velocity, nD. The mean axial velocity is calculated at the quotient of the flow rate over the cross sectional area, minus the shaft or hub area.

Thrust breakdown and cavitation relations

Torque, head rise, and efficiency levels are cavitation dependent. Under highly cavitating conditions, torque, head rise and efficiency diminish. The point when these quantities drop off is called thrust breakdown; the phase "thrust breakdown" is a misnomer since thrust not a consideration. Thrust breakdown is defined by either a 3% drop in head rise or 1% drop in efficiency. A 1% drop in torque is another thrust breakdown criteria, but it only occurs at very low pressures – pressures not tested by RRNMI, therefore it is omitted from comparison discussion. The percent declines are related to the baseline torque, head rise, and efficiency at non-cavitating conditions. The cavitation coefficient is documented throughout breakdown and is expressed as

$$N^* = \frac{p_{t3} - p_v}{\rho\, n^2 D^2} = \frac{g \cdot NPSH}{n^2 D^2} \tag{11}$$

where p_v is the vapor pressure. The term $NPSH$ is an acronym for net positive suction head and is given by

$$NPSH = \frac{p_{t3} - p_v}{\rho g} \tag{12}$$

Hereafter, head rise-related and efficiency-related thrust breakdown is simply called head rise breakdown and efficiency breakdown respectively.

Instrumentation systems

Flow rate

Flow rate is measured at the RRHRC by ducting the exhaust flow outside the tunnel to a MagMaster[TM] electromagnetic flow meter from ABB Kent-Taylor. The flow meter is calibrated using a weight tank. This metering device[6] and calibration technique are superior to those of NSWCCD, and are believed to have a flow rate accuracy of $\pm0.2\%$ over the range of 0 to 1.5 m^3/s. The operating range of the flow meter constrained RRNMI from testing at higher shaft speeds because the maximum flow rate of 1.5 m^3/s would have been exceeded. The NSWCCD used the bellmouth as an orifice-type flow meter, and related flow rate to the pressure difference between the taps upstream and downstream of the contraction. The flow rate to pressure relationship was calibrated to inflow velocity measurements from line surveys from the hub to the casing. Velocimetry readings at a given radial location were assumed to be the circumferential average. This assumption was verified in previous tests in the 36-inch VPWT where PIV measurements indicated the inlet flow was axisymmetric. NSWCCD's flow rate accuracy is $\pm0.7\%$ over the tested range.

Pressure measurements

Static pressure measurements of primary importance are those at the inlet, station 3, and at the nozzle, station 6. Pressures at station 7 are also collected because of concerns of irregular pressures at the nozzle plane. Both RRNMI and NSWCCD used four taps per station, spaced evenly around the circumference, for all stations. At RRNMI, taps at each station coalesce into a manifold. The head rise across the pump is measured by a single differential pressure transducer referenced between the manifold pressures of station 3 and 7. NSWCCD connects each tap to an individual differential pressure transducer with reference to the test section static pressure. Head rise is determined from the difference between the mean pressures at station 3 and 6. The accuracy of the RRNMI and NSWCCD head rise measurements is $\pm1.0\%$ and $\pm0.5\%$, respectively.

Torque and rpm

NSWCCD measure rotor torque with a shaft dynamometer mounted roughly 2 feet upstream of the rotor, whereas RRNMI measures torque with a dynamometer internal to the rotor hub. At NSWCCD, a bladeless rotor is turned to identify the erroneous torque that comes from hub friction; this torque value is subtracted from all subsequent measurements. RRNMI dynamometer arrangement is intended to eliminate effects of the bearing and seal friction, and therefore does not require tare values. The accuracy of the NSWCCD dynamometer is about $\pm0.3\%$ and RRNMI dynamometer has an accuracy of $\pm0.2\%$. NSWCCD determines rpm using a magnetic pickup directed at a 60 tooth gear on the tunnel drive shaft, accurate to about ±1 rpm. RRNMI measures shaft speed with a 720 pulse per revolution Scancon encoder, its accuracy is unknown.

<u>Velocity measurements</u>

RRMNl used a 3-hole pitot probe to measure velocities at stations 3, 6, and 7. At each station, a line survey was made at 8 locations across one radius – from the shaft centerline, or hub surface, to the casing. The mean spacing in the radial direction was $\Delta r/R = 0.101$ at station 3, and $\Delta r/R = 0.0875$ at stations 6 and 7. NSWCCD measured station 3 in a radial line survey using a two-component LDV system. There were 28 measurements, clustered near the shaft surface and casing wall, with a mean spacing of $\Delta r/R = 0.0243$. NSWCCD measured station 6 with a three-component LDV system 629 measurement point array. The array was distributed across the outlet within the z-dimension of $z/R = 0.386$ to -0.522. Within the measurement domain, the mean spacing in the y- and z-direction was $\Delta y/R = 0.0378$ and $\Delta z/R = 0.0534$. The accuracy of NSWCCD measurements at stations 3 and 6 is 0.5% of the total velocity.

Results and discussion

Powering performance

Waterjet powering performance in terms of H^* versus Q^* is shown in Figure 5; H^*_{corr} versus Q^* is shown in Figure 6. A plot of P^* versus Q^* is shown in Figure 7. When comparing the un-corrected results, the head and powering coefficient values for a given flow coefficient are nearly identical between RRNMI and NSWCCD; the RRNMI data points are within the NSWCCD uncertainty band for H^* (1.53% at $Q^* = 0.85$). Roughly 75% of RRNMI data points fall just outside the NSWCCD uncertainty band for P^* (0.3% across the range of Q^*). The uncorrected head coefficient values of RRNMI stem from total head measurements between stations 3 and 7, whereas NSWCCD measure between stations 3 and 6. Station 6, for the NSWCCD setup, is located about 3 rotor radii downstream from the fore face of the rotor, and station 7 in the RRNMI setup is 4.8 rotor radii downstream of the rotor. There is an additional head loss incurred between stations 6 and 7, resulting in comparatively underrated head coefficients of RRNMI. Plots of η^* and η^*_{corr} versus Q^* appear in Figure 8 and Figure 9 respectively. The pump efficiency of the RRNMI waterjet is slightly lower than the efficiency measured by NSWCCD; the difference in efficiency across the range of Q^* is within 2%, but on average is about 1%. The NSWCCD has an uncertainty in η that increases slightly with flow rate, but at $Q^* = 0.85$, the uncertainty measures about 2.11%.

There is not a common correction method since NSWCCD corrects using an energy non-uniformity factor, β_E, whereas RRNMI corrects using another procedure – the exact details and calculations of which are unknown. The differences in the corrections make comparisons difficult. The corrected head coefficients, H^*_{corr}, of RRNMl

8

are greater in value than those of NSWCCD, for a given Q^*. The disparity in H^*_{corr} between RRNMI and NSWCCD grows with flow rate, with a 1.8 % difference at $Q^* = 0.72$ to 3.0 % difference at $Q^* = 0.85$. Comparing one head correction scheme of a given institute's results, over flow rate coefficients of $Q^* = 0.71$ to 0.93, the percent increase in H^*_{corr} over H^* rises from 0.8% to 2.1% for NSWCCD. Over this same flow coefficient interval, RRNMI corrected values grow from 2.9% to 7.3%. Based on these percentages, RRNMI correction scheme increases the H^*_{corr} curve over H^* curve uniformly across all flow coefficients by a factor of 3.5, compared to increases calculated by NSWCCD. The correction RRNMI makes is based on the estimated displacement thickness at the inlet and the swirl at the nozzle. However, the swirl in the outlet is small, with swirl angles rarely greater than ±5°. The author questions how accurate and repeatable are RRNMI swirl-related corrections when swirl is measured across a coarse line survey. RRNMI's correction factor includes a static pressure correction. RRNMI measures head rise between stations 3 and 7, with a static pressure correction added to emulate the head rise between stations 3 and 6. The static pressure correction is somehow related to the static pressure loss incurred between station 6 and 7, believed to be calculated using the canonical Colebrook friction factor relations. As flow rate increases the static pressure loss increases, seemingly increasing this correction factor. Note that a higher flow rate results in a higher Reynolds number flow, based on outlet diameter. Higher Reynolds number pipe flows are associated with a reduction in the friction factor. However, the pressure loss incurred is equal to the product of the friction factor and the square of the mean axial velocity – as the flow rate increases, the reduction in the friction factor is smaller in magnitude than the square of the velocity increase and subsequently the static pressure drop increases. The estimated static pressure drop from stations 6 to 7, for $Q^* = 0.67$, is 0.10 psi (0.71 kPa); at $Q^* = 0.87$ the drop amounts to 0.15 psi (1.08 kPa). This estimate was found using the Colebrook equation, assuming a smooth relative roughness of $\varepsilon/D = 0$, and length between stations 6 and 7 of 8.50 in. (0.216 m.). The static pressure drop is equivalent in magnitude as the differences in RRNMI's corrected head rise and non-corrected head rise, and therefore believed to be the driving factor of all the correction variables. If there was greater swirl in the exhaust flow of the ONR AxWJ-2, it would be expected that this static pressure correction would have a lesser effect on the correction when combined with the swirl correction. It is interesting to point out that in this case of the relatively swirl-less nozzle flows of the ONR AxWJ-2, the correction factor of RRNMI is attributed to a static pressure drop across a length of duct rather than nonuniformities and swirl appearing in a given cross section of the flow, as is the case of the NSWCCD correction procedure. NSWCCD's calculation of the energy non-uniformity factor at the inlet and outlet was $\beta_{E3} = 1.01$ and $\beta_{E6} = 1.016$

Efficiency should increase with Reynolds number based on the writings of Balje[7] and Gulich[8]. Balje indicates that efficiency scales based on the relationship given by

$$\frac{1-\eta_{full}}{1-\eta_{model}} = 0.5 + 0.5\left(\frac{Re_{model}}{Re_{full}}\right)^{0.2} \tag{12}$$

RRNMI results (taken as $Q^* = 0.80$ and $\eta_\beta = 90.7$) scaled to NSWCCD's conditions would result in an efficiency of 91.6, based on either Re_{inlet} or Re_{rotor}. Similarly, RRNMI's and NSWCCD's findings scale to full-scale would predict efficiencies of 93.2 and 91.1 respectively, based on Re_{rotor} where $Re_{rotor\,full\,scale} = 8\cdot10^7$.

The maximum flow rate at RRNMI is limited by the flow meter operating range of $Q_j = 0.150$ m^3/s, which is approached during powering tests, reaching a maximum of $Q_j = 0.149$ m^3/s. The limit of the flow meter effectively limited rotor speed to 1200 rpm. Reynolds number, based on rotor tip speed, would have shown greater similitude between the NSWCCD and RRNMI waterjet had RRNMI tested around 1850 rpm for powering tests.

The head rise coefficient and related total head calculations maybe sensitive to measurement location. NSWCCD and RRNMI stated that inflow measurements of the inlet where measured right at station 3. This corresponds to a normalized position of $x = -1$, and a normalized hub diameter of 0.3. However, RRNMI measurement were recorded at $x = -0.96$, but more importantly the hub diameter at that location is only a normalized value of 0.19. The resulting larger cross sectional area lends to a slower mean axial velocity of roughly 6% (ignoring RRNMI corrections). NSWCCD measurements at station 3 indicated a normalized hub diameter of 0.31, giving a faster mean axial velocity of 1%. Naturally, the static pressure would compensate, with higher pressures associated with slower velocities and vice versa; the total head at a given station would therefore be unaffected by differences in cross sectional area.

Thrust breakdown

Thrust breakdown plots of head rise and efficiency are shown in Figure 10. Efficiency breakdown occurs at decreasing cavitation coefficients as flow rate increases. RRNMI and NSWCCD report nearly identical results of efficiency breakdown, between $Q^* = 0.70$ to 0.80, the gap is roughly 7% in terms of the cavitation coefficient. This difference between RRNMI and NSWCCD grows slight to about 12% at the design point of $Q^* = 0.85$. Head rise breakdown occurs at lower cavitation coefficients than efficiency breakdown, for a given flow rate. Head rise breakdown, opposite in trend to efficiency breakdown occurs at increasing cavitation coefficients as flow rate increases. The difference between efficiency and head rise breakdown amounts to about a 30% difference in the cavitation coefficients at $Q^* = 0.70$ and shrinks to a 10% difference in the cavitation coefficients at $Q^* = 0.85$.

For thrust breakdown experiments, RRNMI ran tests at slower shaft speeds than those of NSWCCD, 1350 rpm compared to 2000 rpm respectively. The slower shaft speeds retard cavitation inception for the same net

positive suction head. Meaning, RRNMI would have to significantly reduce the tunnel pressure to achieve the same cavitation coefficients achieved by NSWCCD. While the higher shaft speeds of the NSWCCD waterjet initiate cavitation at comparatively higher tunnel pressures; with a greater range to reduce the tunnel pressure, NSWCCD could map thrust breakdown to the lowest cavitation coefficients.

Flow measurements

The flow measurements of RRNMI and NSWCCD are illustrated in Figure 11, showing the location of each institutes measurements and the number of measurements per location. Notice that measurements at a particular station, are often situated at slightly different axial locations. Measurements at the inlet, station 3, are shown in Figure 12, 13, and 14. A total of eight velocity surveys at different flow rates were measured by NSWCCD, but only three of those are shown. The local axial, u_x and tangential, u_t velocities are normalized by the mean axial velocity across the inlet, U_{x3}. The relatively smaller shaft diameter of the RRNMI waterjet allowed measurements at a radial location of $r/R = 0.30$, a location interior to NSWCCD's shaft. RRNMI's shaft radius is equal to $r/R = 0.19$, whereas NSWCCD shaft radius is equivalent to $r/R = 0.32$. The difference in inlet geometry did not cause significant discrepancies in the nondimensional axial velocities, results of RRNMI and NSWCCD overlay each other. The RRNMI measurements are of sparse density to capture the velocity gradients near the shaft and casing walls, and fail to capture the shaft and casing boundary layers. Outside of the boundary layers, NSWCCD results were uniformly 1.0 % greater than the mean axial velocity across 85 % of the radial distance. Regardless of the flow coefficient, the axial velocity contours show the same radial profile. The tangential velocities and the swirl angles measured in the inlet are relatively low and indicate that the inflow behavior is almost entirely in the axial direction. The swirl angles reported by NSWCCD average about 1.40°, swirling in the direction of the rotor rotation, across the entire radial cut, for all flow rates. RRNMI indicated similar trends in swirl angles averaging about 0.75° for all radial measurements and for every flow rate condition. The difference in tangential velocities and swirl angles between RRNMI and NSWCCD are within the uncertainty of the measurements; furthermore the magnitudes of the tangential velocities and swirl angles are equal in magnitude to their respective uncertainty.

Measurements of the waterjet outlet, station 6 and 7 are shown in Figure 15, 16, and 17; as before, u_x and u_t are normalized by U_{x3}. NSWCCD measurements at station 6 lay slightly downstream of RRNMI measurements of stations 6; the difference in normalized axial location is 0.40 rotor radii. The difference in location prompted plotting RRNMI measurements at station 7 in order to straddle NSWCCD results; RRNMI's station 7 is about 1.50 rotor radii downstream of NSWCCD's station 6. Unless specifically stated, only RRNMI's station 6 results are discussed. Between radial locations $r/R = 0.1$ and 0.65, NSWCCD indicate a modest rise in axial velocity from $1.90 \cdot U_{x3}$ to $2.05 \cdot U_{x3}$, for both flow rate conditions of $Q^* = 0.85$ and 0.94. RRNMI reported a relative flat

trend across this same radial distance averaging about $2.00 \cdot U_{x3}$ for the flow rates $Q^* = 0.69$, 0.78, and 0.87. From the shaft centerline to $r/R = 0.1$, there is a velocity defect caused by the wake of the stator hub. The flow along the stator hub is quick to recover, with the slowest velocities at the centerline of about $1.4 \cdot U_{x3}$ to $1.65 \cdot U_{x3}$. Smaller wake defects are observed at higher flow rates, but the wake half widths remain about the same. Tangential velocities at the nozzle indicate an inner vortex core surrounded by counter-swirling annular, centered about the shaft centerline. The inner core rotates opposite in direction to the rotor and radiates out to $r/R = 0.15$. From there to $r/R = 0.40$ is the annular flow pattern swirling in the same direction as the rotor. The smaller inner core has higher magnitude tangential velocities than the wider annular. The tangential velocity magnitudes within the inner core decrease with increasing flow rate. Conversely, tangential velocities in the annular increase with decreasing flow rate. RRNMI results at $Q^* = 0.87$ show similar trends with NSWCCD results at $Q^* = 0.85$ and 0.94. At the lower flow rates tested by RRNMI of $Q^* = 0.69$ and 0.78, the inner core and annular take up a larger fraction of the outlet cross section. RRNMI measurements do not have sufficient resolution to capture the strength of the inner core. RRNMI results did not indicate the zero tangential velocity at the centroid of the inner core, $r/R = 0.00$. This problem may be traced to the large sensing volume of the RRNMI 3-hole pitot probe or misalignment of the probe. RRNMI measurements at the flow rate condition $Q^* = 0.69$, indicate that off the design point of $Q^* = 0.85$, tangential velocities magnitudes are amplified. RRNMI measurements at $Q^* = 0.69$, represent the slowest flow over the stator blades in terms of streamwise velocity and stator blade Reynolds number. For slow stator flows, the stator would be less effective in countering the swirl of the rotor. The nozzle flow would have flow patterns with tangential velocities and swirl angles orientated in the rotation of the rotor. Swirl angles are plotted in Figure 17, and show identical trends to the tangential velocity curves.

Cavitation performance

The nature and degree of rotor cavitation was recorded on photographs and video by RRNMI and NSWCCD. Cavitation was observed over a range of flow rates and tunnel pressures. Figure 18 illustrates the camera locations in the RRNMI and NSWCCD setup. Also shown in Figure 18 is the relative rotor position of the RRNMI and the NSWCCD waterjet during image capture; the rotor positions vary by an estimated 28 degrees. Figure 19 shows comparisons of the side view photographs. RRNMI photographs focus on one particular rotor blade, making it easier to observe trends by eliminating blade-to-blade variation. NSWCCD viewed several blades, but blade variation was not apparent. Tip-related cavitation from the RRNMI observations occurs at the quater-chord section and precipitates about the tip separation vortex. The wedge-shaped cavitation region is characterized by the following: 1) a relatively small area, 2) forms a shallow angle between its upstream boundary and the local blade tangent, of about 8°, and 3) its fore boundary is defined by the edge of the tip and the suction

side of the blade – it does not persist to the peripheral blade surface, between the tip and the casing. Comparatively, tip-related cavitation for the NSWCCD rotor initiates at the mid-chord on the edge defining the tip and the pressure side. The cavitation region rounds the tip to the suction side, driven by a strong leakage flow, and grows in intensity at it follows the tip-leakage vortex. The large tangential velocities of the tip leakage jet flare the wedge-shaped cavitation region to an angle of 12°, relative to the tangent blade surface, to cover a greater area. The ensuing tip-leakage vortex is greater in magnitude than the separation vortex.

The differences between the tip cavitation indicate that the tip gap of the NSWCCD waterjet is relatively larger than that of RRNMI. Inone et al.[9], You et al.[10], and Goto[11] have found that an increase in the tip gap shifts the origin of the tip-leakage vortex downstream and increases the vorticity. They too observed an increase angle between the tip-leakage vortex center and the blade, which is also congruent to the findings of Muthanna and Devenport[12] and Wang and Devenport[13]. The difference in cavitation inception index is expected to increase with tip gap size.

The difference in the inflow casing boundary layer thickness may also be a factor. The bellmouth geometry may affect the inflow boundary layers on the casing. The relative velocity between the rotor tip and the slow moving flow along the casing would be exceedingly high, and worsen with thicker boundary layers. Thicker boundary layers cause greater tip loading and more susceptible conditions for tip cavitation. Tip cavitation would then occur at relatively higher tunnel pressures and could cause cavitation closer to the leading edge.

Figure 20 are suction side photographs of the RRNMI and NSWCCD waterjet. RRNMI located the camera at an oblique angle to the inlet resulting in an impaired view of the suction side surfaces; whereas NSWCCD provide images directly normal to the top most blade. RRNMI show a noticeable amount of variability between rotor blades worsened by the non-uniformity in illumination between the top and bottom sections of the rotor. The top starboard rotor blade tends to cavitate in a region confined to the tip; the lower starboard rotor cavitates noticeably more, encompassing the outer half of the blade span. Suction side cavitation occurs in a predicable manner for NSWCCD. The cavitation region initiates at the leading edge at a span of $r/R = 0.85$. With the exception of the highest flow rate condition, $Q* = 0.85$, and cavitation numbers, $N* = 1.54$ and 1.93, suction side cavitation occurred for all tests.

Conclusion

The two independent tests by RRNMI and NSWCCD provided a unique opportunity into how facilities measure waterjet performance. A direct comparison between results of the institutes was mildly hampered by several factors. Naturally, the difference in waterjet size, shaft speeds, and mean axial velocities lead to scaling-related discrepancies; the dissimilarity in rotor blade Reynolds number is the key aspect. It is difficult to quantify how rotor blade Reynolds number alters results. In another sense, it is desirable to have different scales ratios as it fulfills the greater need to show trends between model-scale and full-scale. Rotor tip clearance is a highly sensitive variable in waterjet performance. RRNMI's slightly smaller tip clearance, compared to NSWCCD's, is believed to provide greater head rise, efficiency, and also lessen tip leakage. The difference in normalized measurement location caused disparities in head rise, and to a lesser concern, swirl. For shorter distances in the axial direction between inlet and nozzle measurements, head rise will increase. Caution is needed when applying friction factor relations as a means of accounting for differences in measurement location and head rise, since swirl in the nozzle flow may skew results. Measurements further downstream of the nozzle will have reduced swirl. Greater transparency in RRNMI's head correction procedure would aid in making comparisons between the corrected results. The dissimilarity in correction procedures of RRNMI and NSWCCD illustrates a need for a common correction technique.

Table 1: Specifications and dimensions of the AxWJ-2 and geosyms tested by RRNMI and NSWCCD.

Specification	AxWJ-2	
Rotor blade number	6	
Stator blade number	8	
Inlet area to nozzle area ratio	1.85	
Length from inlet to nozzle, l/D	3	
Specified hub diameter at inlet, d_{hub}/D	0.3	
Rotor chord at 0.7 r/R, c/D	0.7612	
Design Q^*	0.85	
Approximate model scale η^*	90%	

Specification	RRNMI - ONR AxWJ-2	NSWCCD – ONR AxWJ-2
Inlet diameter, feet (meters)	0.6561 (0.2000)	1.000 (0.3048)
Nozzle diameter, feet (meters)	0.4593 (0.1400)	0.700 (0.2133)
Rotor		
Rotor diameter, feet (meters)	0.6546 (0.1995)	0.998 (0.3042)
Tip gap, feet (meters)	0.0008330 (0.0002540)	0.001667 (0.0005080)
Tip gap to rotor dia. ratio	0.001270	0.001667
Bellmouth,		
Maximum diameter, feet (meters)	~1.14 (~0.35)	3.000 (0.9144)
Length fore of inlet, feet (meters)	~0.46 (~0.14)	2.500 (0.762)
Hub fairing		
Shape	Straight taper	Straight taper
Minimum diameter, feet (meters)	~0.15 (~0.047)	0.3000 (0.09144)
Maximum diameter, feet (meters)	0.1968 (0.06000)	0.3229 (0.09842)
Diameter at station 3, feet (meters)	~0.17 (~0.054)	0.300 (0.09144)
Length, feet (meters)	~0.26 (~0.080)	0.8229 (0.2508)
Additions	Exhaust ducting with auxiliary pump and flow meter	Three nozzle extensions at 80%, 90% and 100% of nozzle diameter

Table 2: Summary of test programs of the RRNMI and NSWCCD.

Powering tests

Institute	Q_i (ft^3/s)	Q^*	n (r/min)	$Re_{inlet} \cdot 10^6$	$Re_{blade} \cdot 10^6$	Q (ft-lb)	P_d (hp)	P^*	H^*
NSWCCD	16.6-21.8	0.71-0.93	1400	2.53-3.47	4.66-5.15	339-356	90.4-95.0	2.02-2.12	1.78-2.60
RRNMI	3.72-5.25	0.65-0.92	1200	0.67-0.95	1.39-1.48	31.5-32.0	6.99-7.32	2.03-2.13	1.79-2.67

Cavitation observations

Institute	Q^*	N^*	Photo/Video locations
NSWCCD	0.711-3.285	0.757-0.830	Front view, side view
RRNMI	0.650-0.850	1.25-2.07	Front view, side view, nozzle, outlet

Flow surveys

Institute	station	type	points	locations	Q^*	$Re_{inlet} \cdot 10^6$	Equipment
NSWCCD	3	Line survey	28	$(x,\text{theta}) = (-1, 120°)$	0.71-0.94	4.66-4.83	2D-LDV
	4	Line survey	55	$(x,\text{theta}) = (0, 120°)$	0.71, 0.77, 0.85	4.66-4.83	3D-LDV
	6	Flow field	629	$(x, y, z) = (2.55, -0.5-0.8, -1,1)$	0.85-0.94	4.83-4.96	3D-LDV
RRNMI	3	Line survey	8	$(x,\text{theta}) = (-0.96, 0°)$	0.69, 0.78, 0.87	1.40-1.46	3-hole probe
	6	Line survey	8	$(x,\text{theta}) = (2.66, 0°)$	0.69, 0.78, 0.87	1.40-1.46	3-hole probe
	7	Line survey	8	$(x,\text{theta}) = (3.82, 0°)$	0.69, 0.78, 0.87	1.40-1.46	3-hole probe

Breakdown

Institute	Q^* at N^* 1%	Q^* at H^* 3%
NSWCCD	0.71-0.84	0.70-0.83
RRNMI	0.65-0.85	0.65-0.85

Table 3: Dimensional performance results, in standard units, of RRNMI tests.

Q_l	n	Q	P_d	ΔP_{stat}	ΔP_{dync}	$\Delta P_{\beta\,dync}$	H	H_{corr}	ΔH
(ft^3/s)	(r/min)	(lb$_f$ft)	(hp)	(psi)	(psi)	(psi)	(psi)	(psi)	(% diff)
3.727	1200	31.51	7.197	3.680	2.527	2.680	6.207	6.360	2.465
3.901	1200	31.81	7.271	3.347	2.769	2.936	6.116	6.283	2.731
3.983	1200	31.92	7.295	3.185	2.886	3.060	6.070	6.245	2.883
4.073	1200	31.96	7.303	2.951	3.017	3.200	5.968	6.151	3.066
4.149	1200	32.03	7.318	2.752	3.131	3.321	5.883	6.073	3.230
4.154	1200	32.03	7.320	2.746	3.139	3.329	5.885	6.075	3.229
4.155	1200	32.02	7.318	2.742	3.140	3.330	5.882	6.073	3.247
4.240	1200	32.01	7.312	2.479	3.270	3.468	5.748	5.946	3.445
4.241	1200	32.04	7.321	2.492	3.272	3.470	5.764	5.963	3.452
4.319	1200	32.03	7.316	2.246	3.394	3.599	5.639	5.845	3.653
4.323	1200	32.03	7.318	2.246	3.399	3.605	5.646	5.852	3.649
4.324	1200	32.02	7.314	2.250	3.400	3.606	5.650	5.856	3.646
4.403	1200	31.96	7.302	1.985	3.526	3.740	5.511	5.725	3.883
4.408	1200	32.03	7.317	1.999	3.534	3.748	5.533	5.748	3.886
4.487	1200	31.94	7.298	1.747	3.661	3.883	5.409	5.631	4.104
4.490	1200	31.90	7.289	1.736	3.668	3.890	5.404	5.626	4.108
4.492	1200	31.91	7.289	1.719	3.670	3.892	5.389	5.612	4.138
4.573	1200	31.87	7.281	1.477	3.805	4.035	5.281	5.512	4.374
4.576	1200	31.87	7.280	1.465	3.809	4.040	5.275	5.506	4.379
4.664	1200	31.77	7.258	1.174	3.957	4.197	5.131	5.371	4.677
4.664	1200	31.79	7.262	1.185	3.957	4.197	5.143	5.382	4.647
4.746	1200	31.64	7.229	0.905	4.098	4.346	5.002	5.250	4.958
4.748	1200	31.65	7.232	0.920	4.100	4.349	5.020	5.268	4.940
4.835	1200	31.49	7.194	0.626	4.252	4.509	4.878	5.135	5.269
4.835	1200	31.51	7.198	0.637	4.252	4.509	4.889	5.146	5.257
4.918	1200	31.33	7.157	0.341	4.399	4.666	4.741	5.007	5.611
4.922	1200	31.36	7.164	0.354	4.407	4.674	4.761	5.027	5.587
5.082	1200	31.01	7.084	-0.233	4.698	4.983	4.465	4.749	6.361
5.086	1200	31.00	7.081	-0.246	4.705	4.990	4.459	4.743	6.369
5.253	1200	30.62	6.995	-0.851	5.019	5.323	4.169	4.471	7.244

Table 4: Dimensional performance results, in metric units, of RRNMI tests.

Q_i	n	Q	P_d	ΔP_{stat}	ΔP_{dync}	$\Delta P_{\beta\,dync}$	H	H_{corr}	ΔH
(m³/s)	(r/sec)	(N·m)	(kW)	(kPa)	(kPa)	(kPa)	(kPa)	(kPa)	(% diff)
0.1056	20.00	42.72	5.367	25.37	17.42	18.48	42.80	43.85	2.465
0.1105	20.01	43.13	5.422	23.08	19.09	20.24	42.16	43.32	2.731
0.1128	20.01	43.28	5.440	21.96	19.90	21.10	41.85	43.06	2.883
0.1153	20.00	43.33	5.446	20.35	20.80	22.06	41.15	42.41	3.066
0.1175	20.00	43.43	5.457	18.97	21.59	22.90	40.56	41.87	3.230
0.1176	20.01	43.43	5.459	18.93	21.64	22.95	40.57	41.89	3.229
0.1177	20.01	43.42	5.457	18.91	21.65	22.96	40.56	41.87	3.247
0.1201	20.00	43.40	5.453	17.09	22.54	23.91	39.63	41.00	3.445
0.1201	20.00	43.45	5.459	17.18	22.56	23.92	39.74	41.11	3.452
0.1223	20.00	43.42	5.456	15.48	23.40	24.82	38.88	40.30	3.653
0.1224	20.00	43.43	5.457	15.49	23.44	24.86	38.93	40.35	3.649
0.1224	20.00	43.41	5.454	15.51	23.44	24.86	38.96	40.38	3.646
0.1247	20.00	43.33	5.445	13.68	24.31	25.79	38.00	39.47	3.883
0.1248	20.00	43.42	5.456	13.79	24.37	25.84	38.15	39.63	3.886
0.1270	20.00	43.31	5.442	12.05	25.24	26.77	37.29	38.82	4.104
0.1272	20.00	43.26	5.435	11.97	25.29	26.82	37.26	38.79	4.108
0.1272	20.00	43.26	5.436	11.85	25.30	26.83	37.16	38.69	4.138
0.1295	20.00	43.21	5.429	10.18	26.23	27.82	36.41	38.00	4.374
0.1296	20.00	43.20	5.429	10.10	26.26	27.86	36.37	37.96	4.379
0.1321	20.00	43.07	5.412	8.09	27.28	28.93	35.38	37.03	4.677
0.1321	20.00	43.10	5.416	8.17	27.28	28.94	35.46	37.11	4.647
0.1344	20.00	42.90	5.391	6.24	28.25	29.96	34.49	36.20	4.958
0.1344	20.00	42.92	5.393	6.34	28.27	29.98	34.61	36.32	4.940
0.1369	20.00	42.69	5.365	4.32	29.31	31.09	33.63	35.40	5.269
0.1369	20.00	42.72	5.368	4.39	29.32	31.09	33.70	35.48	5.257
0.1393	20.00	42.47	5.337	2.35	30.33	32.17	32.69	34.52	5.611
0.1394	20.00	42.52	5.343	2.44	30.39	32.23	32.83	34.66	5.587
0.1439	20.00	42.04	5.282	-1.61	32.39	34.35	30.79	32.74	6.361
0.1440	20.00	42.02	5.281	-1.70	32.44	34.40	30.74	32.70	6.369
0.1488	20.00	41.51	5.216	-5.86	34.61	36.70	28.74	30.82	7.244

Table 5: Dimensional performance results, in standard units, of NSWCCD tests; only 33 data points are represented of the 67 data points set.

Q_i (ft^3/s)	n (r/min)	Q (lb_fft)	P_d (hp)	ΔP_{stat} (psi)	ΔP_{dync} (psi)	$\Delta P_{\beta\,dync}$ (psi)	H (psi)	H_{corr} (psi)	ΔH (% diff)
16.60	1400	353.6	94.28	10.116	8.94	9.10	19.06	19.22	0.839
16.63	1400	354.2	94.43	10.052	8.98	9.14	19.03	19.19	0.841
16.84	1400	354.1	94.40	9.644	9.22	9.38	18.86	19.02	0.848
17.00	1401	354.6	94.57	9.358	9.39	9.55	18.74	18.91	0.907
17.28	1401	355.2	94.73	8.775	9.69	9.87	18.47	18.64	0.920
17.49	1400	354.8	94.60	8.324	9.93	10.11	18.25	18.43	0.986
17.69	1401	355.2	94.73	7.879	10.15	10.33	18.03	18.21	0.998
17.94	1401	354.9	94.64	7.342	10.44	10.62	17.78	17.97	1.069
18.05	1401	354.9	94.64	7.076	10.56	10.75	17.64	17.83	1.077
18.19	1401	354.9	94.63	6.756	10.73	10.92	17.48	17.67	1.087
18.34	1401	354.6	94.57	6.432	10.91	11.10	17.34	17.53	1.096
18.46	1401	354.4	94.51	6.159	11.05	11.25	17.21	17.41	1.162
18.77	1401	353.3	94.22	5.429	11.42	11.63	16.85	17.06	1.246
18.98	1400	354.4	94.48	4.952	11.66	11.87	16.61	16.82	1.264
19.35	1400	353.0	94.11	4.068	12.13	12.35	16.20	16.42	1.358
19.37	1400	353.1	94.14	4.023	12.15	12.37	16.17	16.39	1.361
19.38	1400	352.3	93.91	4.022	12.16	12.37	16.18	16.40	1.360
19.53	1400	352.6	94.00	3.640	12.34	12.56	15.98	16.20	1.377
19.60	1400	352.4	93.97	3.471	12.44	12.67	15.92	16.14	1.382
19.65	1400	351.7	93.76	3.363	12.50	12.73	15.86	16.09	1.450
19.79	1400	351.5	93.72	3.031	12.67	12.89	15.70	15.93	1.465
19.91	1401	351.1	93.64	2.723	12.83	13.06	15.55	15.78	1.479
19.97	1400	351.1	93.62	2.584	12.91	13.14	15.49	15.72	1.485
20.13	1400	350.0	93.31	2.173	13.12	13.35	15.29	15.53	1.570
20.22	1401	350.0	93.35	1.942	13.23	13.47	15.17	15.41	1.582
20.36	1400	349.0	93.06	1.585	13.42	13.66	15.00	15.25	1.667
20.59	1400	347.6	92.67	1.019	13.71	13.96	14.73	14.97	1.629
20.70	1400	346.4	92.32	0.664	13.87	14.12	14.53	14.78	1.721
20.89	1400	345.9	92.24	0.209	14.11	14.37	14.32	14.58	1.816
20.98	1400	345.1	91.96	-0.042	14.24	14.49	14.19	14.45	1.832
21.16	1400	344.0	91.73	-0.514	14.48	14.74	13.97	14.23	1.861
21.46	1400	341.9	91.13	-1.346	14.90	15.17	13.55	13.82	1.993
21.63	1400	340.7	90.84	-1.803	15.12	15.39	13.32	13.59	2.027

Table 6: Dimensional performance results, in metric units, of NSWCCD tests; only 33 data points are represented of the 67 data points set.

| Q_j (m³/s)	n (r/sec)	Q (N·m)	P_d (kW)	ΔP_{stat} (kPa)	ΔP_{dync} (kPa)	$\Delta P_{\beta\,dync}$ (kPa)	H (kPa)	H_{corr} (kPa)	ΔH (% diff)
0.4699	23.34	479.5	70.30	69.75	61.65	62.75	131.4	132.5	0.839
0.4708	23.34	480.2	70.42	69.31	61.90	63.01	131.2	132.3	0.841
0.4770	23.34	480.1	70.39	66.49	63.53	64.67	130.0	131.2	0.848
0.4815	23.35	480.8	70.52	64.52	64.71	65.87	129.2	130.4	0.907
0.4894	23.35	481.5	70.64	60.50	66.84	68.03	127.3	128.5	0.920
0.4953	23.34	481.0	70.54	57.39	68.45	69.67	125.8	127.1	0.986
0.5009	23.35	481.6	70.64	54.33	70.00	71.25	124.3	125.6	0.998
0.5080	23.34	481.2	70.57	50.62	71.96	73.25	122.6	123.9	1.069
0.5111	23.34	481.2	70.58	48.79	72.84	74.14	121.6	122.9	1.077
0.5150	23.34	481.2	70.57	46.58	73.96	75.28	120.5	121.9	1.087
0.5193	23.34	480.8	70.52	44.35	75.19	76.54	119.5	120.9	1.096
0.5228	23.34	480.5	70.48	42.46	76.18	77.55	118.6	120.0	1.162
0.5316	23.34	479.0	70.26	37.43	78.76	80.17	116.2	117.6	1.246
0.5373	23.34	480.5	70.46	34.15	80.38	81.82	114.5	116.0	1.264
0.5480	23.34	478.7	70.18	28.05	83.63	85.13	111.7	113.2	1.358
0.5486	23.33	478.8	70.20	27.74	83.76	85.26	111.5	113.0	1.361
0.5487	23.34	477.6	70.03	27.73	83.82	85.32	111.5	113.1	1.360
0.5530	23.34	478.0	70.10	25.10	85.09	86.62	110.2	111.7	1.377
0.5551	23.34	477.8	70.08	23.93	85.80	87.34	109.7	111.3	1.382
0.5564	23.34	476.8	69.92	23.18	86.19	87.74	109.4	110.9	1.450
0.5603	23.34	476.6	69.89	20.90	87.34	88.90	108.2	109.8	1.465
0.5637	23.34	476.1	69.83	18.77	88.45	90.03	107.2	108.8	1.479
0.5655	23.34	476.1	69.81	17.82	89.00	90.60	106.8	108.4	1.485
0.5701	23.34	474.5	69.58	14.98	90.43	92.06	105.4	107.0	1.570
0.5725	23.34	474.6	69.61	13.39	91.20	92.84	104.6	106.2	1.582
0.5767	23.34	473.2	69.40	10.93	92.52	94.18	103.4	105.1	1.667
0.5829	23.34	471.2	69.11	7.03	94.52	96.22	101.5	103.2	1.629
0.5863	23.33	469.7	68.84	4.58	95.62	97.34	100.2	101.9	1.721
0.5915	23.34	469.0	68.78	1.44	97.31	99.06	98.8	100.5	1.816
0.5940	23.33	467.8	68.58	-0.29	98.15	99.91	97.9	99.6	1.832
0.5993	23.34	466.4	68.40	-3.54	99.86	101.66	96.3	98.1	1.861
0.6078	23.33	463.5	67.96	-9.28	102.72	104.57	93.4	95.3	1.993
0.6124	23.34	462.0	67.74	-12.43	104.24	106.11	91.8	93.7	2.027

Table 7: Non-dimensional performance results of RRNMI tests.

| Q^*	P^*	H^*	H_{corr}^*	ΔH^* (% diff)	η (%)	η_{corr} (%)	$\Delta \eta$ (% diff)
0.6598	2.099	2.679	2.743	2.389	84.13	86.27	2.544
0.6903	2.117	2.637	2.707	2.655	85.87	88.30	2.830
0.7047	2.124	2.617	2.691	2.828	86.73	89.30	2.963
0.7206	2.127	2.573	2.650	2.993	87.08	89.82	3.147
0.7344	2.133	2.538	2.618	3.152	87.27	90.16	3.312
0.7350	2.131	2.537	2.617	3.153	87.38	90.28	3.319
0.7351	2.131	2.536	2.617	3.194	87.38	90.29	3.330
0.7504	2.132	2.480	2.564	3.387	87.20	90.29	3.544
0.7507	2.134	2.487	2.571	3.378	87.37	90.46	3.537
0.7645	2.133	2.433	2.520	3.576	87.11	90.37	3.742
0.7652	2.133	2.435	2.523	3.614	87.26	90.53	3.747
0.7653	2.132	2.437	2.525	3.611	87.38	90.65	3.742
0.7793	2.128	2.377	2.468	3.828	86.95	90.41	3.979
0.7801	2.133	2.387	2.478	3.812	87.21	90.67	3.967
0.7941	2.127	2.333	2.428	4.072	86.99	90.65	4.207
0.7948	2.125	2.331	2.426	4.076	87.10	90.77	4.214
0.7950	2.125	2.325	2.420	4.086	86.88	90.56	4.236
0.8095	2.122	2.278	2.377	4.346	86.79	90.67	4.471
0.8100	2.122	2.275	2.374	4.352	86.74	90.63	4.485
0.8255	2.115	2.213	2.316	4.654	86.26	90.38	4.776
0.8256	2.117	2.218	2.321	4.644	86.40	90.53	4.780
0.8401	2.107	2.157	2.264	4.961	85.91	90.27	5.075
0.8403	2.108	2.165	2.272	4.942	86.21	90.58	5.069
0.8557	2.097	2.104	2.214	5.228	85.74	90.37	5.400
0.8558	2.098	2.108	2.219	5.266	85.88	90.51	5.391
0.8705	2.086	2.044	2.159	5.626	85.21	90.10	5.739
0.8712	2.088	2.053	2.168	5.602	85.56	90.45	5.715
0.8996	2.065	1.925	2.048	6.390	83.78	89.22	6.493
0.9002	2.064	1.922	2.045	6.400	83.75	89.20	6.507
0.9298	2.039	1.797	1.928	7.290	81.86	87.93	7.415

Table 8: Non-dimensional performance results of NSWCCD tests; only 33 data points are represented of the 67 data points set.

Q^*	P^*	H^*	H_{corr}^*	ΔH^* (% diff)	η (%)	η_{corr} (%)	$\Delta\eta$ (% diff)
0.7112	2.111	2.607	2.629	0.844	87.84	88.58	0.842
0.7125	2.114	2.603	2.625	0.845	87.73	88.47	0.843
0.7218	2.114	2.580	2.602	0.853	88.11	88.88	0.874
0.7284	2.115	2.562	2.585	0.898	88.23	89.02	0.895
0.7402	2.118	2.524	2.548	0.951	88.22	89.04	0.929
0.7494	2.117	2.496	2.521	1.002	88.35	89.21	0.973
0.7578	2.118	2.465	2.490	1.014	88.16	89.05	1.010
0.7686	2.118	2.431	2.457	1.070	88.24	89.17	1.054
0.7732	2.117	2.412	2.438	1.078	88.08	89.03	1.079
0.7792	2.117	2.391	2.417	1.087	87.97	88.94	1.103
0.7856	2.115	2.370	2.397	1.139	88.03	89.02	1.125
0.7909	2.114	2.353	2.380	1.147	88.01	89.02	1.148
0.8042	2.108	2.304	2.332	1.215	87.91	88.97	1.206
0.8131	2.116	2.273	2.301	1.232	87.34	88.44	1.259
0.8294	2.108	2.217	2.247	1.353	87.21	88.38	1.342
0.8303	2.107	2.212	2.241	1.311	87.16	88.33	1.342
0.8304	2.102	2.213	2.243	1.356	87.41	88.58	1.339
0.8368	2.104	2.186	2.216	1.372	86.93	88.14	1.392
0.8399	2.104	2.177	2.208	1.424	86.93	88.15	1.403
0.8423	2.099	2.167	2.198	1.431	86.98	88.21	1.414
0.8478	2.097	2.146	2.178	1.491	86.76	88.02	1.452
0.8528	2.095	2.127	2.158	1.457	86.56	87.84	1.479
0.8557	2.095	2.119	2.151	1.510	86.53	87.82	1.491
0.8626	2.088	2.091	2.123	1.530	86.38	87.71	1.540
0.8661	2.089	2.075	2.107	1.542	86.03	87.37	1.558
0.8726	2.083	2.052	2.085	1.608	85.96	87.34	1.605
0.8820	2.074	2.014	2.048	1.688	85.66	87.09	1.669
0.8875	2.069	1.989	2.023	1.709	85.33	86.79	1.711
0.8949	2.064	1.958	1.993	1.788	84.92	86.43	1.778
0.8992	2.060	1.942	1.977	1.802	84.77	86.30	1.805
0.9067	2.052	1.910	1.945	1.832	84.40	85.97	1.860
0.9198	2.040	1.854	1.890	1.942	83.57	85.22	1.974
0.9266	2.033	1.821	1.858	2.032	83.00	84.69	2.036
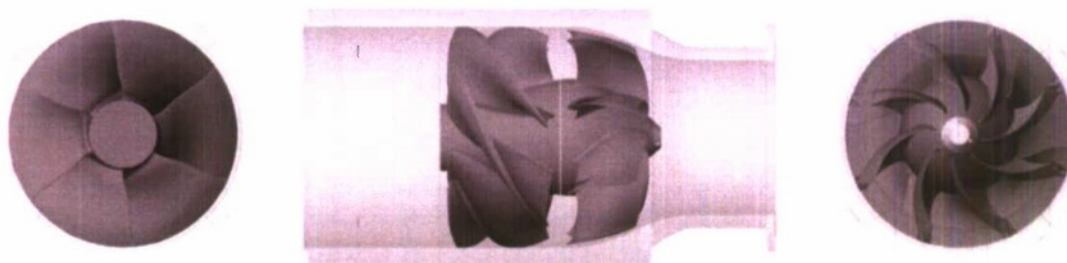
Figure 1. ONR Axial Flow Waterjet 2, ONR AxWJ-2.
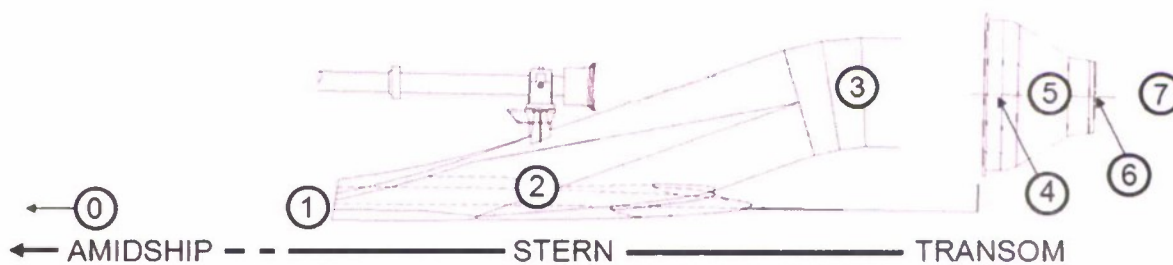

Station No.	Location
0	in undisturbed flow far ahead of the vehicle
1	one inlet diameter forward of inlet tangency point
2	normal to the internal flow at the aft lip of the intake
3	just ahead of the rotor
4	between rotor and stator or between stages
5	behind stator
6	at the nozzle outlet plane
7	behind the nozzle outlet plane

Figure 2: ITTC reference stations are illustrated in the figure above and accompanied with descriptions below.
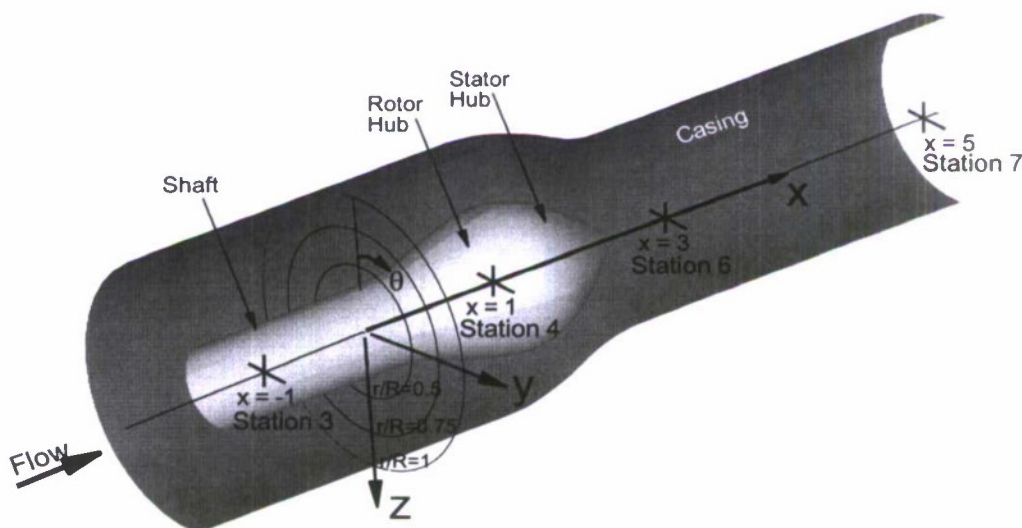
Figure 3: Illustration of waterjet station locations and coordinate system.

(a)

(b)
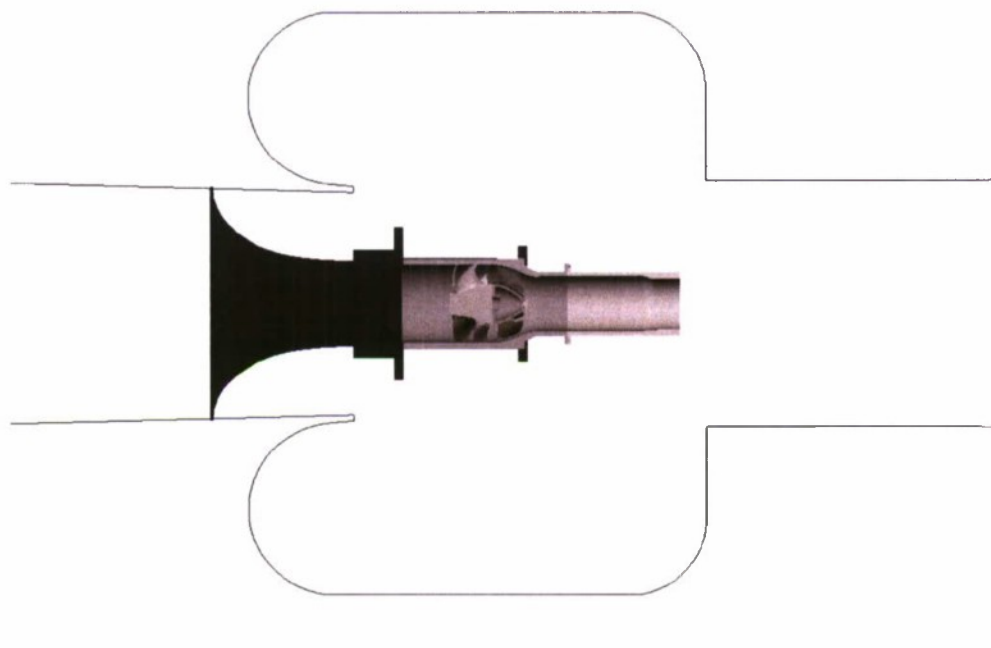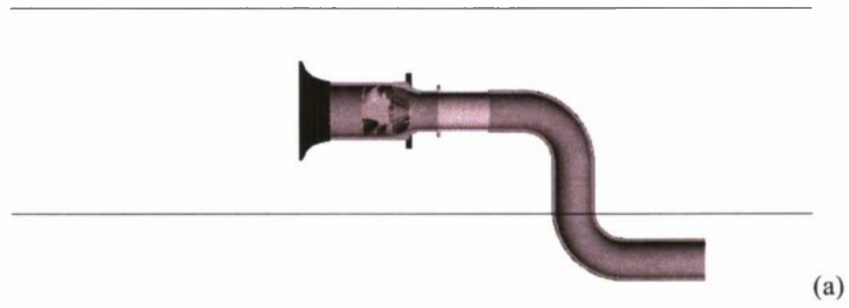
Figure 4: Side view illustration of the test setup at (a) RRNMI and (b) NSWCCD. The relative sizes of the facilities are preserved. Outlining each schematic is a representation of the water tunnel and test section boundaries. The flow is from left to right.
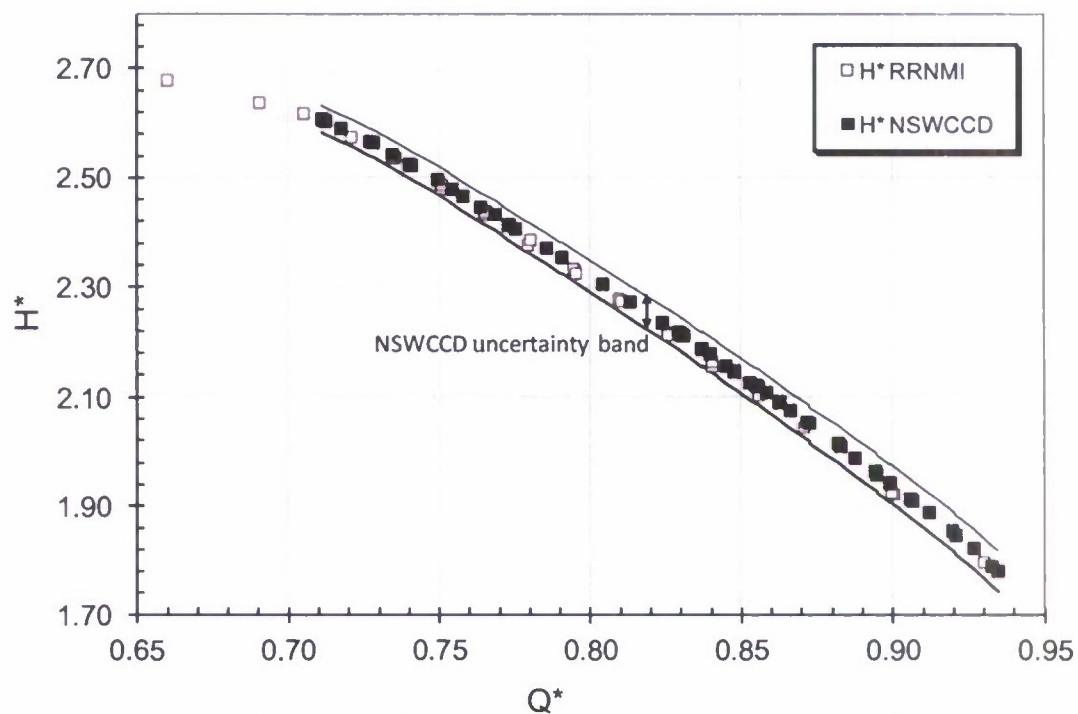
Figure 5: Measured head coefficient versus flow coefficient results.
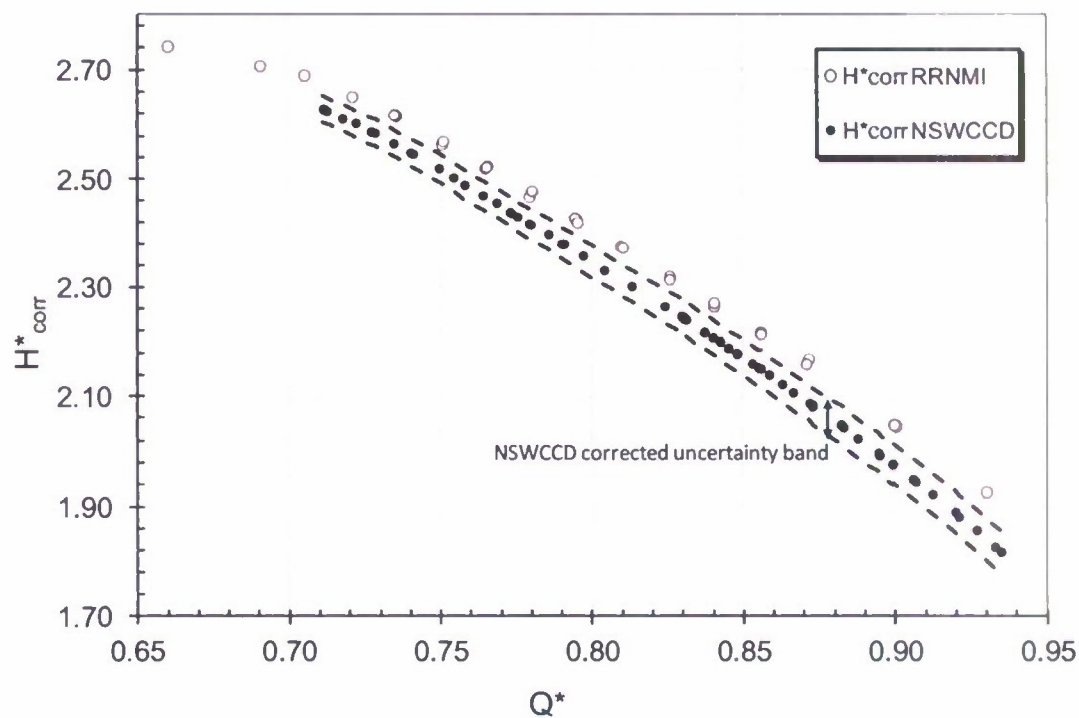
**Figure 6:** Measured corrected head coefficient versus flow coefficient results.
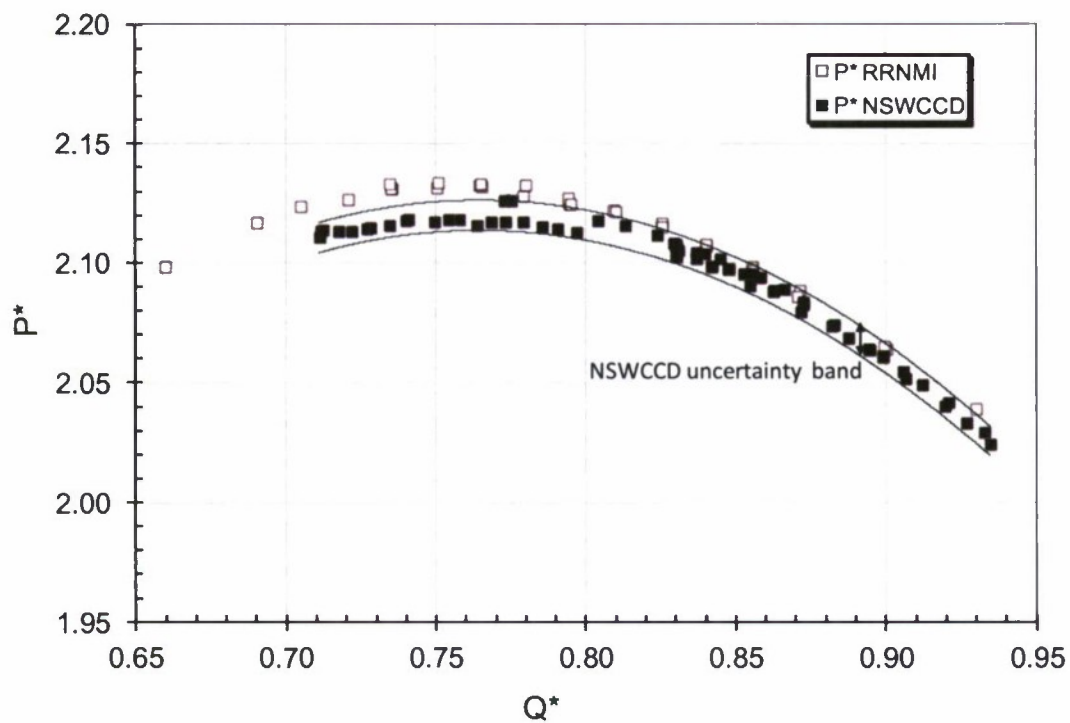
Figure 7: Measured power coefficient versus flow coefficient results.
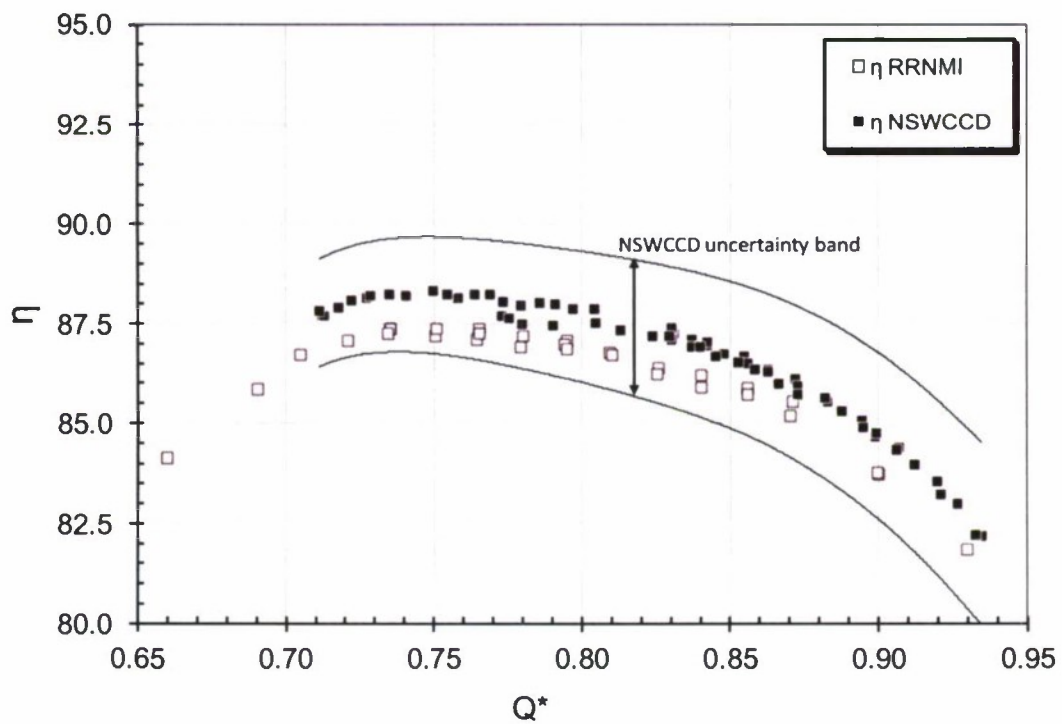
Figure 8: Measured efficiency versus flow coefficient results.
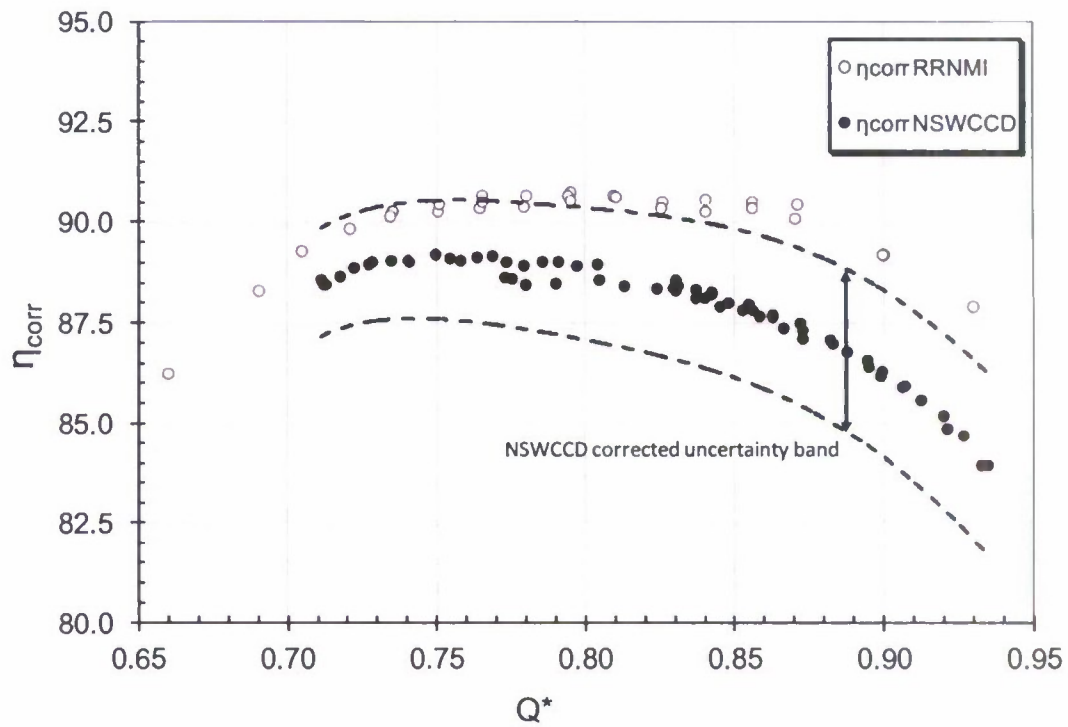
Figure 9: Measured corrected efficiency versus flow coefficient results.
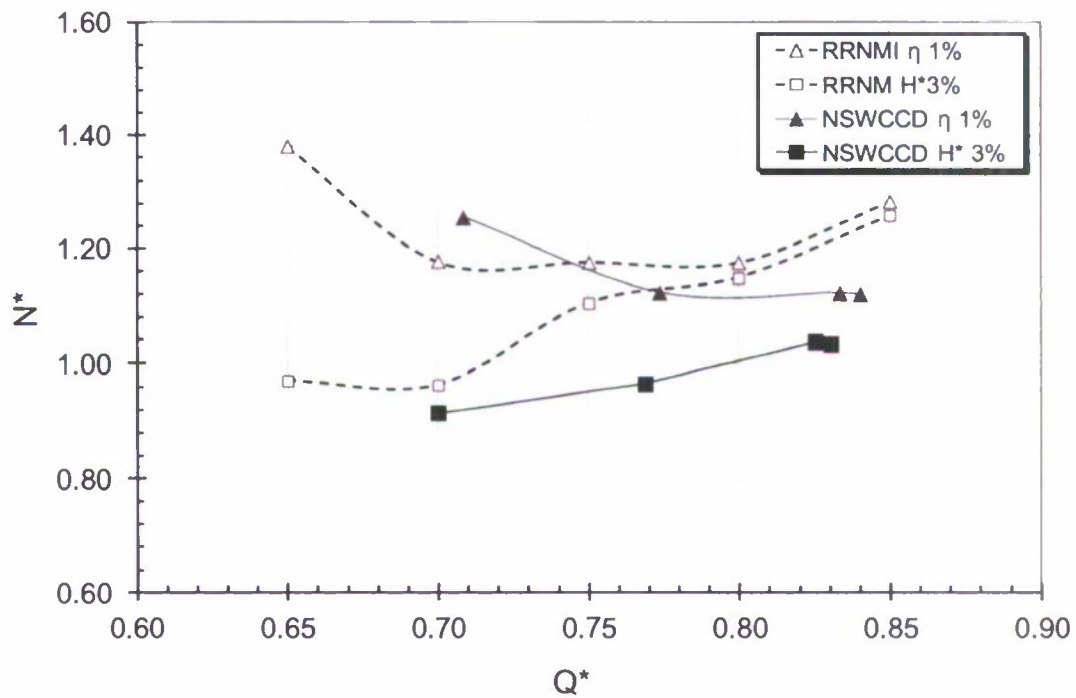
Figure 10: Thrust breakdown versus flow coefficient results.
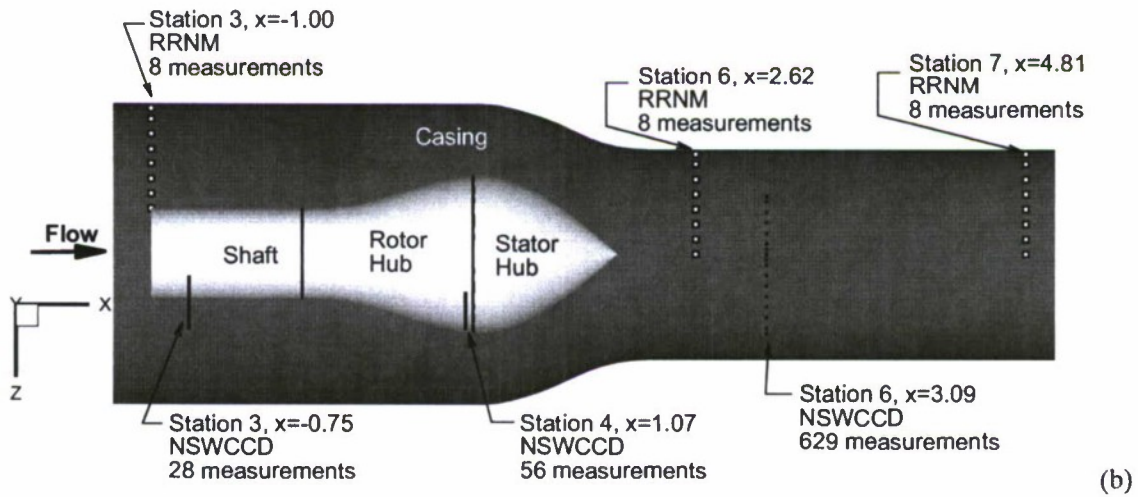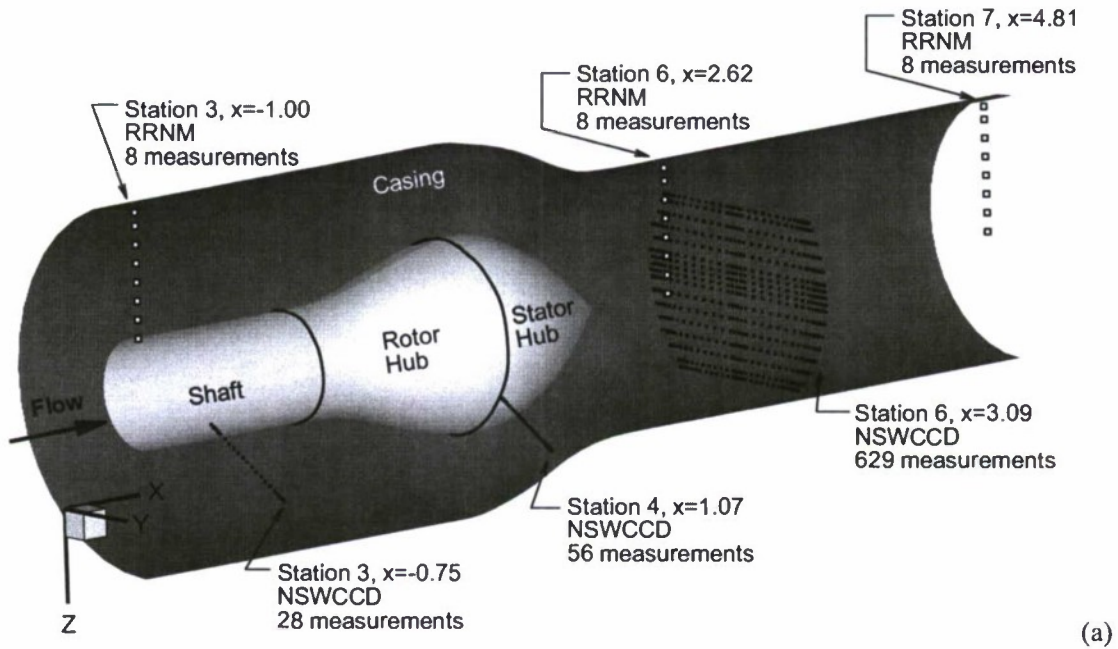
Figure 11: Illustrations from a (a) isometric view and (b) side view of the waterjet showing normalized measurement locations of RRNMI and NSWCCD.
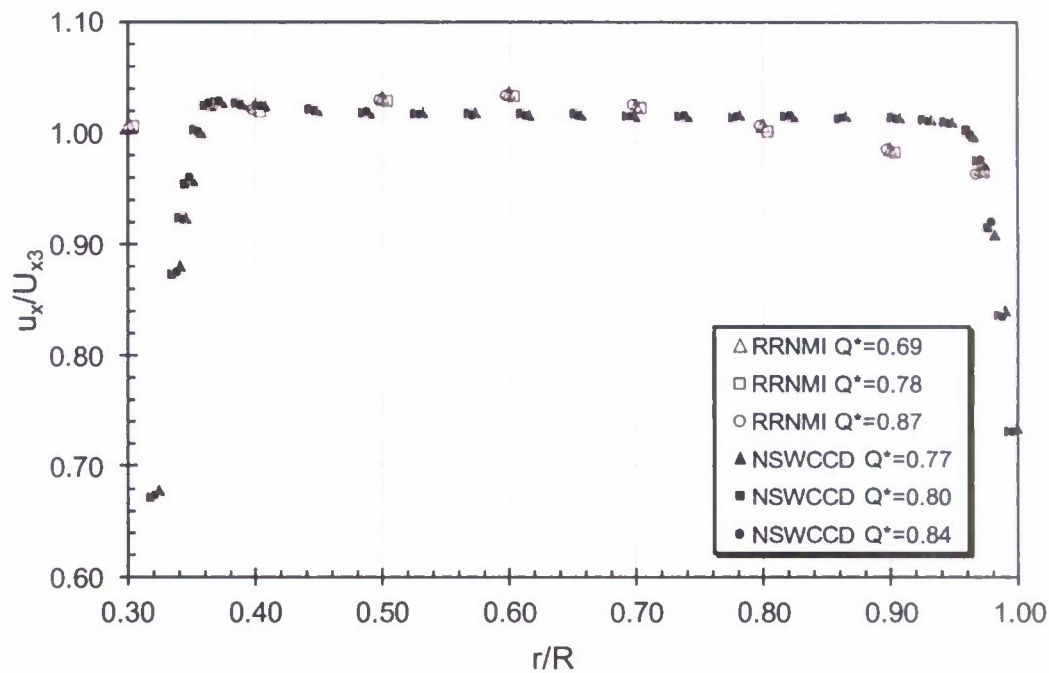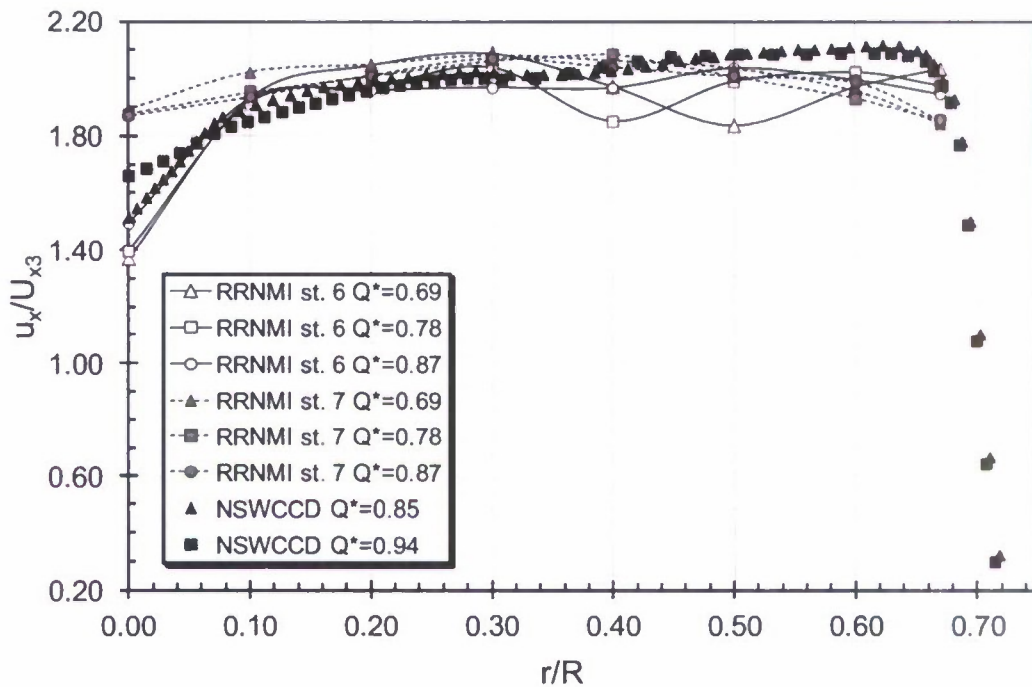
Figure 12: Station 3 - Inflow axial velocity, normalized by the mean axial velocity, U_{x3}, in the radial direction, normalized by the inlet radius.
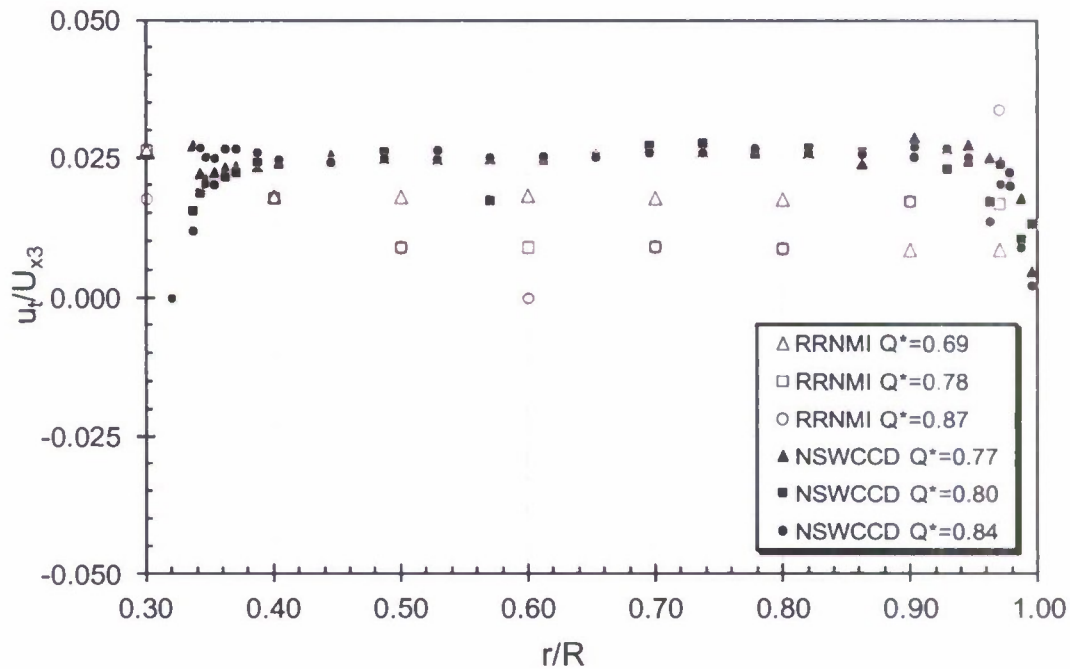
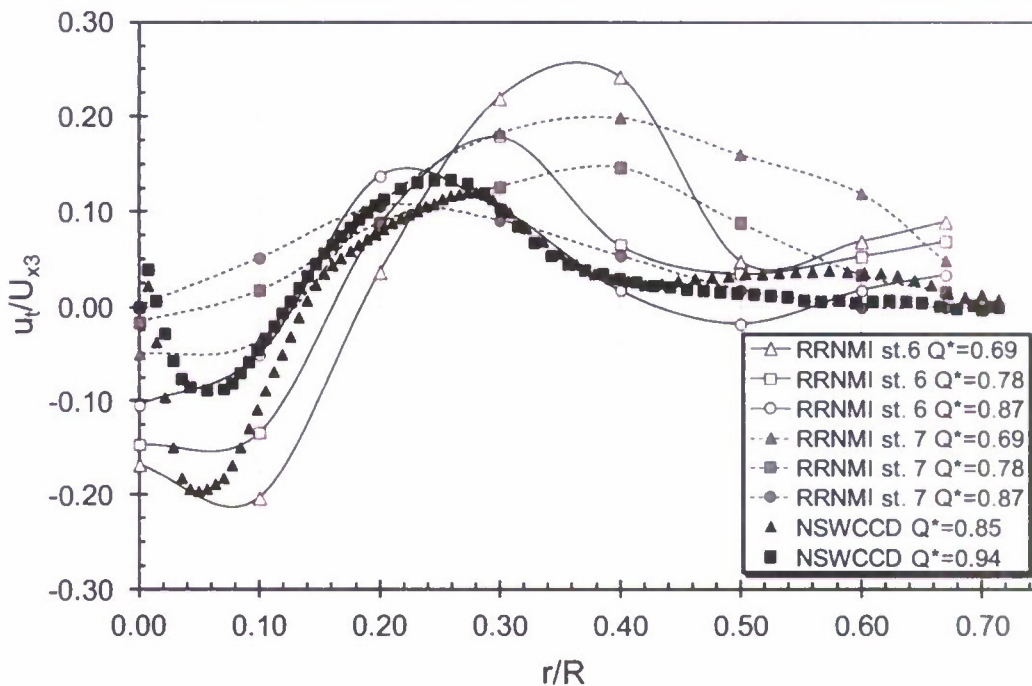**Figure 13:** Station 3 – Inflow tangential velocities, normalized by the U_{x3}, relative to the radial direction.
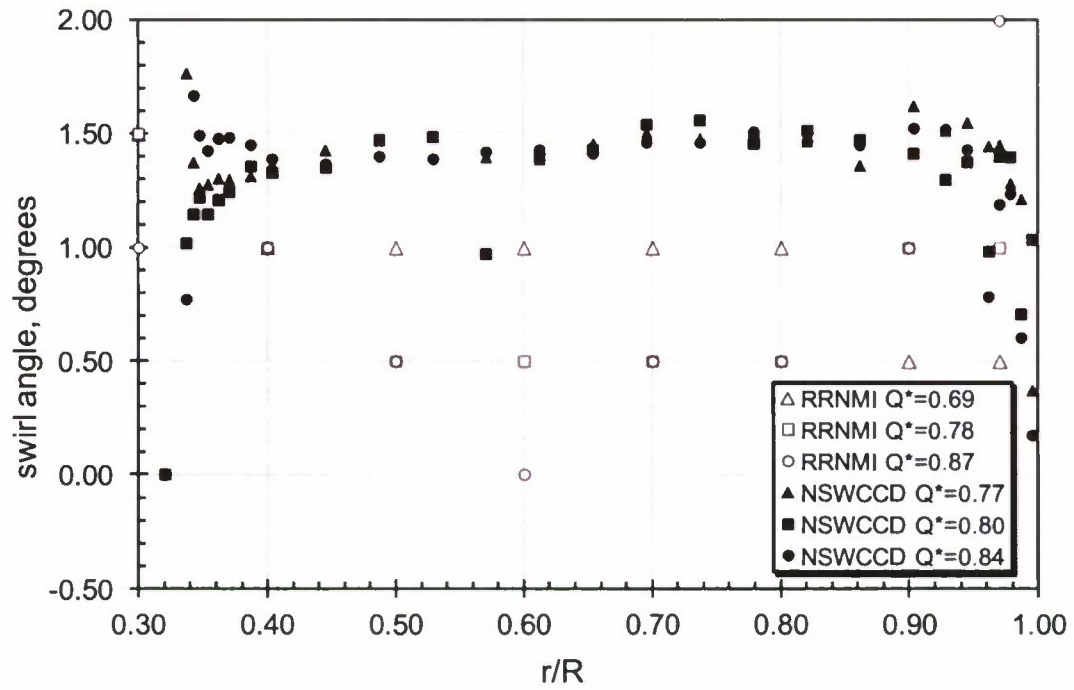
Figure 14: Station 3 – Inflow swirl angles relative to the radial direction.

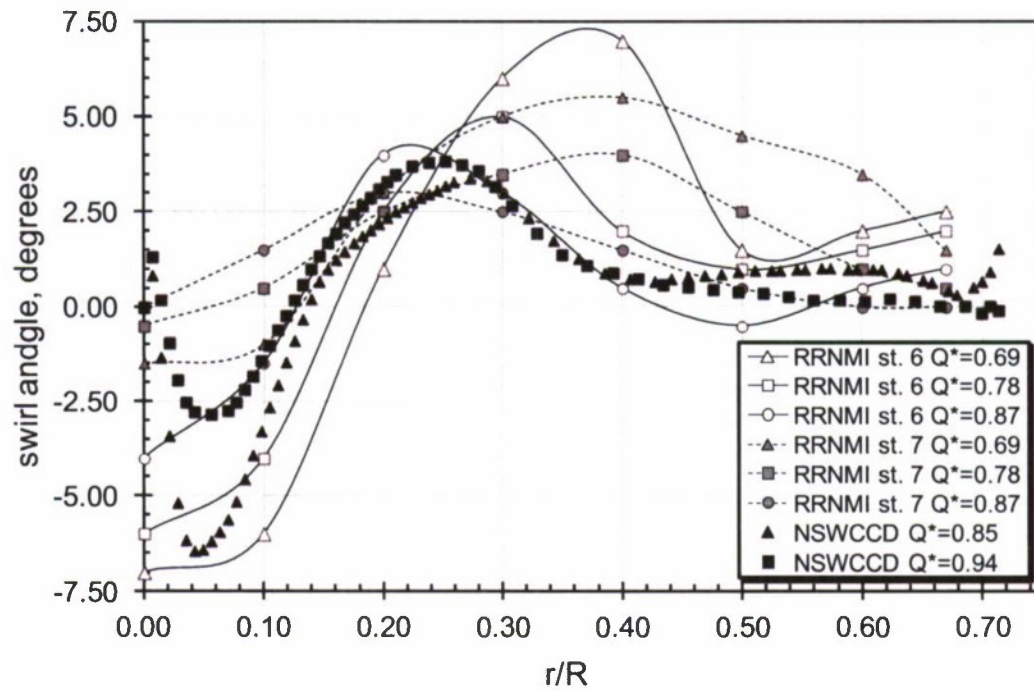**Figure 15:** Station 6 – Axial velocities, normalized by U_{x3}, relative to the radial direction.[*]

*Note: some NSWCCD data points were removed to better distinguish curves

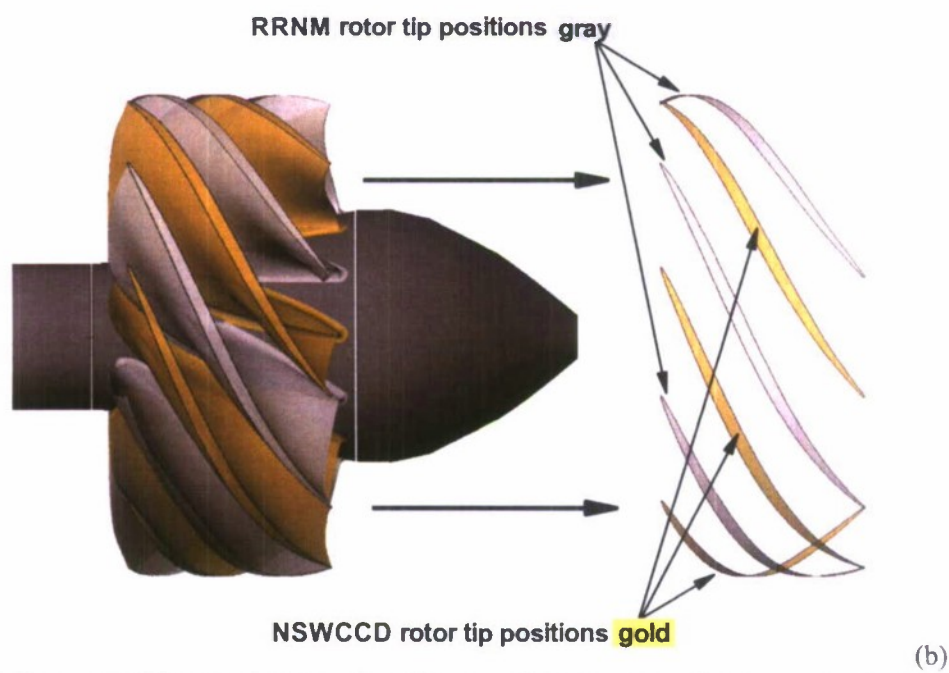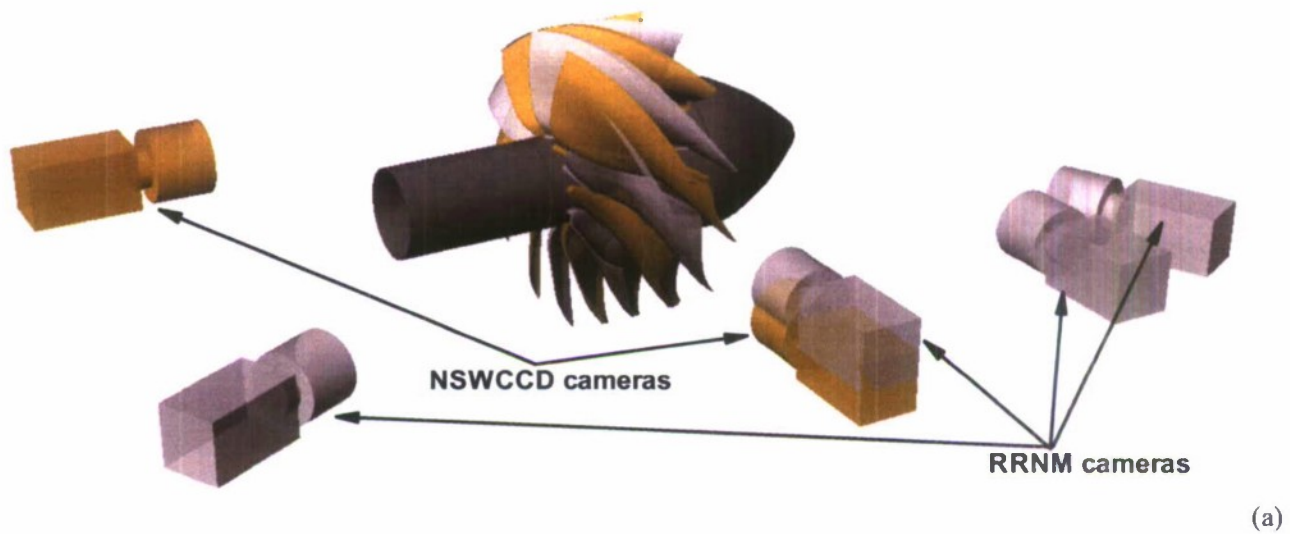**Figure 16:** Station 6 – Tangential velocities, normalized by U_{x3}, relative to the radial direction.[*]

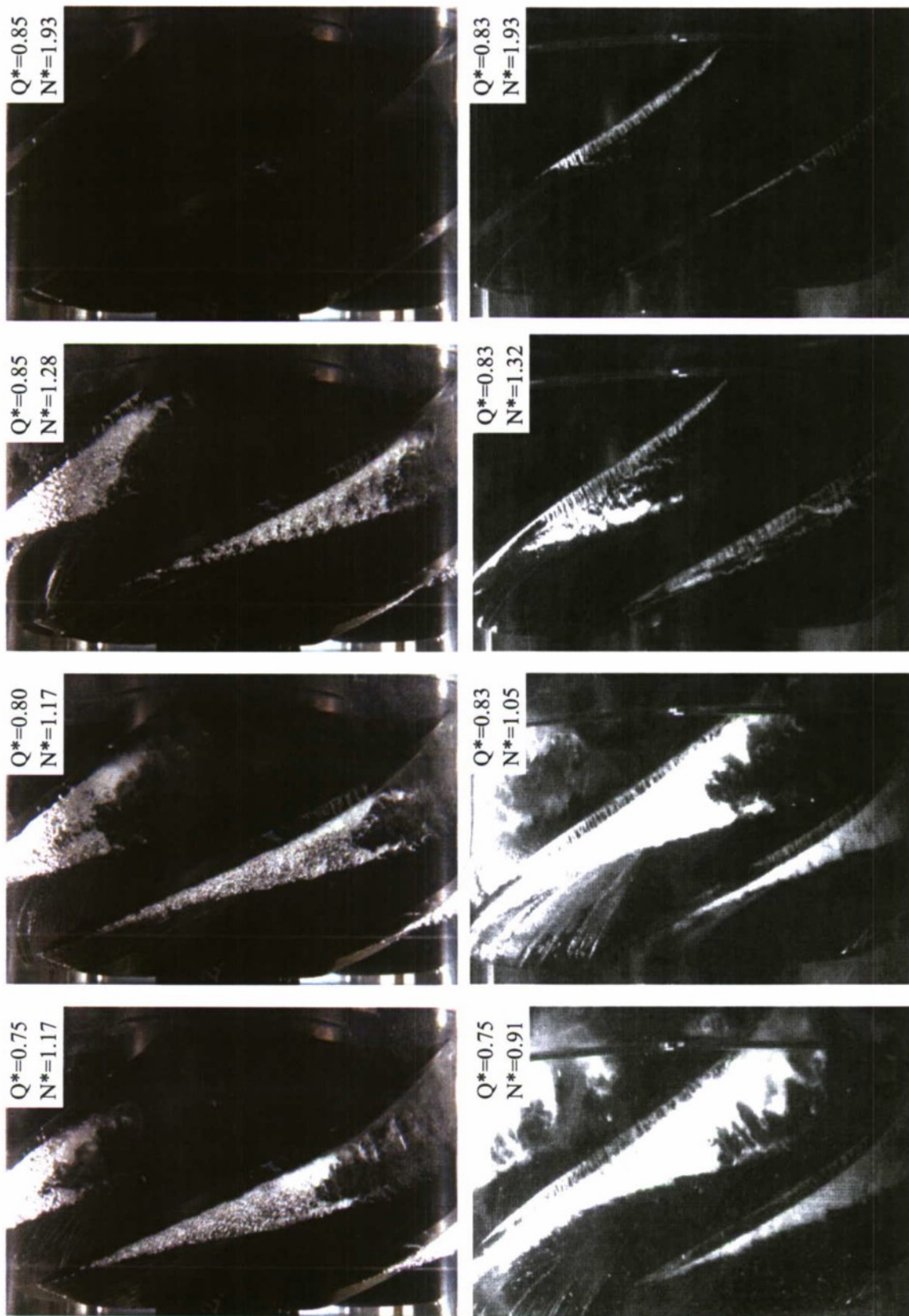*Note: some NSWCCD data points were removed to better distinguish curves

Figure 17: Station 6 – Swirl angle curves relative to the radial direction.*
*Note: some NSWCCD data points were removed to better distinguish curves

(a)

(b)

Figure 18: (a) Camera positions and perspectives shown relative to rotor. (b) The overlaid rotor positions of the RRNMI waterjet and the NSWCCSD waterjet during image capture. The rotor positions are offset by about 28°.

Q*=0.85
N*=1.93

Q*=0.83
N*=1.93

Q*=0.85
N*=1.28

Q*=0.83
N*=1.32

Q*=0.80
N*=1.17

Q*=0.83
N*=1.05

Q*=0.75
N*=1.17

Q*=0.75
N*=0.91

Figure 19: Side views of the RRNMI waterjet (top) and the NSWCCD (bottom), in ascending cavitation coefficient from left to right.
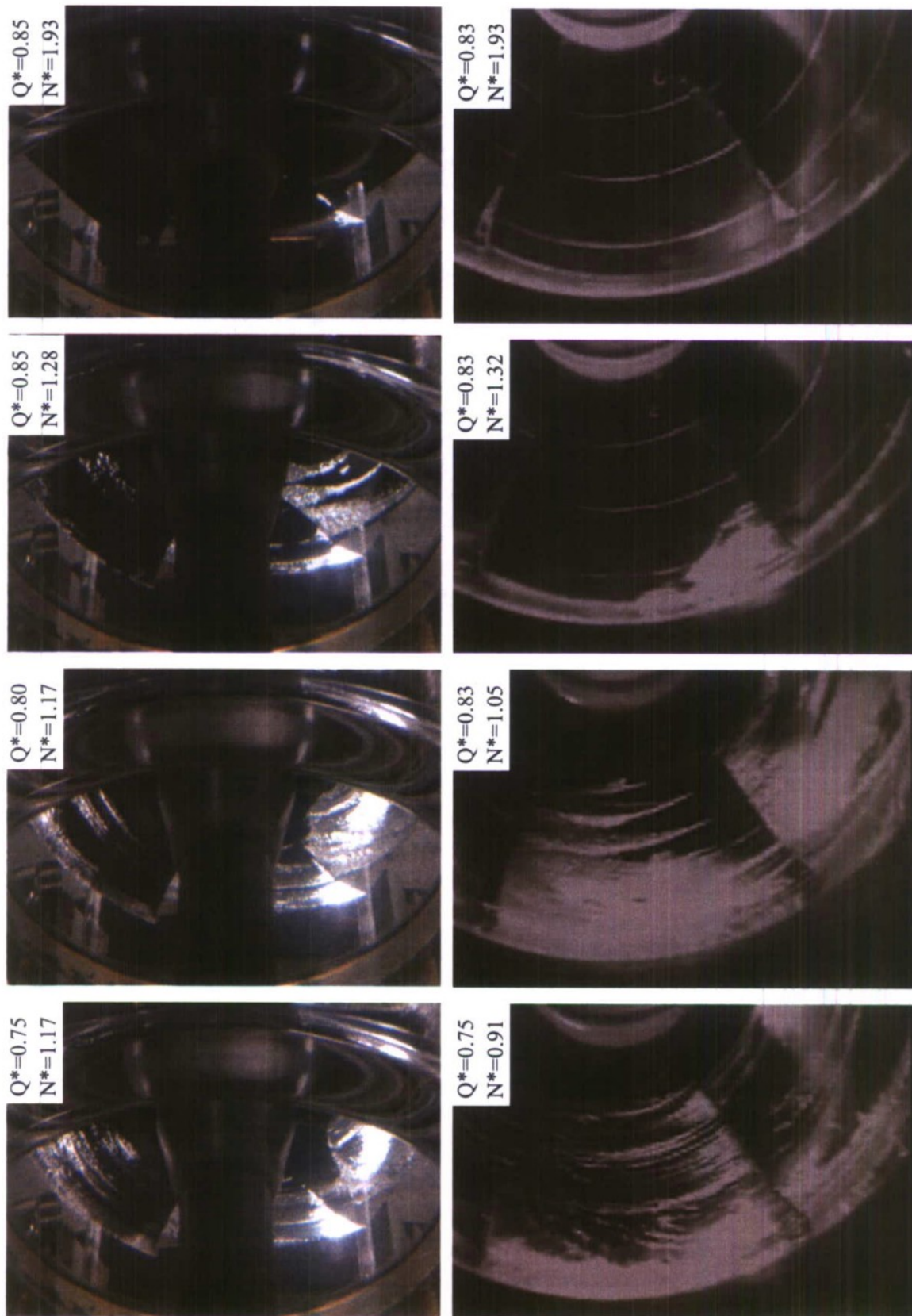
Figure 20: Suction side views of the RRNMI waterjet (top) and the NSWCCD (bottom), in ascending cavitation coefficient from left to right.

Q*=0.75
N*=1.17

Q*=0.80
N*=1.17

Q*=0.85
N*=1.28

Q*=0.85
N*=1.93

Q*=0.75
N*=0.91

Q*=0.83
N*=1.05

Q*=0.83
N*=1.32

Q*=0.83
N*=1.93

References

1. Office of Naval Research, "ONR BAA Announcement # 06-011," Arlington, VA (March 2006).

2. Michael, T. J., Schroeder, S. D., and Becnel, A. J., "Design of the ONR AxWJ-2 Axial Flow Water Jet Pump," NSWCCD-50-TR-2008/066 (November 2008).

3. Chesnakas, C. J., Donnelly, M. J., Pfitsch, D. W., Becnel, A. J., Schroeder, S. D., "Performance Evaluation of the ONR Axial Waterjet 2 (AxWJ-2)," NSWCCD-50-TR-2009/089 (December 2009).

4. Anderson, L., "ONR AxWJ-2, Pump Loop Test," Rolls Royce Hydrodynamic Research Center Report PR-1223, issue 1 (July 2010).

5. ITTC 1996, "ITTC Quality Manual for High Speed Marine Vehicles, Waterjets," 21st International Towing Tank Conference, Bergen and Trondheim (Norway 1996).

6. Quoted from website: MagMaster MFE Series Flowmeters, Electromagnetic Sensors, http://www.wisnercontrols.com/pdfs/CatalogPDFs/Magmaster.pdf.

7. Balje, O. E., Turbomachines: A Guide to Design, Selection and Theory, 1st ed., John Wiley & Sons, New York, NY (1981).

8. Gulich, J. F., Centrifugal Pumps, Springer, New York, NY (2008).

9. Inoue, M., Kuroumaru, M., Fukuhara, M., "Behavior of tip-leakage flow behind an axial compressor rotor," Journal of Engineering: Gas Turbine Power, Vol. 108, no. 7 (1986).

10. You, D., Wang, M., Moin, P., Mittal, R., "Effects of tip-gap size on the tip-leakage flow in a turbomachinery cascade," Physics of Fluids, Vol. 18., no. 105102-1 (2006).

11. Goto, A., "Three-dimensional flow and mixing in an axial flow compressor with different rotor tip clearance," J. Turbomachinery, Vol. 114, p. 765, (1992).

12. Muthanna, C. and Devenport, "Wake of a compressor cascade with tip gap. Part 1. Mean and turbulence structure," AIAA Journal, Vol. 42, p. 2320 (2004).

13. Wang, Y., and Devenport, W. J., "Wake of a compressor cascade with tip gap. Part 2. Effects of endwall motion," AIAA Journal, Vol. 42, p. 2332 (2004).

Initial Distributuion

Organization	Name	Copies
ONR 331	K. Kim	1
NAVSEA 05Z	J. Schumann	2
DTIC		1

CENTER DISTRIBUTION

Code	Name	Copies
3452	NSWCCD Library	pdf only
5030	S. Jessup	1
5060	D. Walden	1
5800	M. Donnelly	1
	R. Hurwitz	pdf only
	Files	2